CELL BIOLOGY

# Autophagy induction in atrophic muscle cells requires ULK1 activation by TRIM32 through unanchored K63-linked polyubiquitin chains

M. Di Rienzo[1,2], M. Antonioli[1], C. Fusco[3], Y. Liu[4], M. Mari[5], I. Orhon[5], G. Refolo[1], F. Germani[1], M. Corazzari[6], A. Romagnoli[1], F. Ciccosanti[1], B. Mandriani[3], M. T. Pellico[3], R. De La Torre[4], H. Ding[7], M. Dentice[8], M. Neri[9], A. Ferlini[9], F. Reggiori[5], M. Kulesz-Martin[4,10], M. Piacentini[1,2]*, G. Merla[3], G. M. Fimia[1,11]*



**Optimal autophagic activity is crucial to maintain muscle integrity, with either reduced or excessive levels leading to specific myopathies. LGMD2H is a muscle dystrophy caused by mutations in the ubiquitin ligase TRIM32, whose function in muscles remains not fully understood. Here, we show that TRIM32 is required for the induction of muscle autophagy in atrophic conditions using both in vitro and in vivo mouse models. Trim32 inhibition results in a defective autophagy response to muscle atrophy, associated with increased ROS and MuRF1 levels. The pro-autophagic function of TRIM32 relies on its ability to bind the autophagy proteins AMBRA1 and ULK1 and stimulate ULK1 activity via unanchored K63-linked polyubiquitin. LGMD2H-causative mutations impair TRIM32's ability to bind ULK1 and induce autophagy. Collectively, our study revealed a role for TRIM32 in the regulation of muscle autophagy in response to atrophic stimuli, uncovering a previously unidentified mechanism by which ubiquitin ligases activate autophagy regulators.**

## INTRODUCTION

Autophagy is a catabolic process that ensures the removal of excess or damaged cellular components in physiological and pathological conditions and provides metabolic supplies when extracellular nutrients are scarce (*1*, *2*). By keeping the intracellular environment free of harmful material, autophagy plays a key protective role in several human diseases (*3*). Hereditary myopathies are among the best-documented examples of the close relationship between dysregulated autophagy and human disorders (*4*). Defective autophagy has been observed in collagen VI–related myopathies, Duchenne muscular dystrophy, and Emery-Dreifuss muscular dystrophy, while impaired recognition of autophagy cargos is present in the limb-girdle muscular dystrophy (LGMD) 1D and in myofibrillar myopathies (*4*, *5*). Conversely, excessive autophagy activation characterizes the merosin-deficient congenital muscular dystrophy 1A (*6*).

Cellular alterations caused by autophagy dysregulation in muscles include the presence of damaged mitochondria and enlarged endoplasmic reticulum, the impaired turnover of sarcomeric proteins, and the increased susceptibility to cell death (*5*). Restoration of appropriate autophagy levels by pharmacological or dietary approaches ameliorates the myopathic defects in mouse models for collagen VI–related and Duchenne muscular dystrophies, providing preclinical evidence of the relevance of dysfunctional autophagy in these diseases (*7*–*9*). These studies have also uncovered the existence of signaling pathways that link autophagy to the proper functioning of muscle cell compartments, such as the extracellular matrix (through collagen VI and laminin-2), cytoskeleton–to–plasma membrane interaction (dystrophin), and nuclear envelope (lamin A/C) (*4*). The mechanisms by which these signals converge to the autophagy machinery to modulate its activity, however, remain unknown.

Tripartite motif-containing 32 (TRIM32) is a member of the TRIM protein family, a large group of E3 ubiquitin ligases characterized by the presence of a RING finger domain, a B-box domain, a coiled-coil region, and a variable C-terminal region (*10*). NHL domains characterized the C terminus of TRIM32, which are involved in protein dimerization and substrate recognitions (*11*). Mutations in the NHL domains of the *TRIM32* are causative of LGMD2H and sarcotubular myopathy, which are mild and severe manifestations of the same disorder (*12*). Both *trim32* knock-out (KO) and knock-in mice carrying a disease-associated mutation have confirmed the myopathic phenotype as a consequence of TRIM32 dysfunction (*13*, *14*) and highlighted the presence of neurological defects that may also contribute to the muscular disorder (*13*). A missense mutation in the B-box domain of TRIM32 causes the Bardet-Biedl syndrome type 11, a disease characterized by obesity, retinal degeneration, genito-urinary tract malformations, and cognitive impairment, but not showing muscle alterations (*15*). In keeping with this observation, TRIM32 also plays a role in the regulation of processes not directly related to muscle function, such as immunity, neural differentiation, and cancer (*16*).

How TRIM32 mutations cause muscular dystrophy has not been entirely clarified. A pro-atrophy role of TRIM32 has been initially postulated on the basis of its ability to ubiquitinate actin, tropomyosin, troponins, α-actinin, and desmin (*17*, *18*). TRIM32 also inhibits the prosurvival phosphatidylinositol 3-kinase/Akt pathway through the

[1]National Institute for Infectious Diseases IRCCS, Lazzaro Spallanzani, 00149 Rome, Italy. [2]Department of Biology, University of Rome, Tor Vergata, 00133 Rome, Italy. [3]Division of Medical Genetics, IRCCS, Casa Sollievo della Sofferenza, 71013 San Giovanni Rotondo, Italy. [4]Department of Dermatology, Oregon Health and Science University, Portland, OR 97239, USA. [5]Department of Biomedical Sciences of Cells and Systems, University of Groningen, University Medical Center Groningen, 9713 AV Groningen, Netherlands. [6]Department of Health Sciences, University of Piemonte Orientale "A. Avogadro", Novara, Novara, Italy. [7]Department of Biochemistry and Medical Genetics, University of Manitoba, Winnipeg, Manitoba, Canada. [8]Department of Clinical Medicine and Surgery, University of Naples Federico II, 80131 Naples, Italy. [9]Section of Medical Genetics, Department of Medical Sciences, University of Ferrara, 44121 Ferrara, Italy. [10]Department of Cell, Developmental and Cancer Biology, Oregon Health and Science University, Portland, OR 97239, USA. [11]Department of Biological and Environmental Sciences and Technologies (DiSTeBA), University of Salento, Lecce 73100, Italy.
*Corresponding author. Email: mauro.piacentini@uniroma2.it (M.P.); gianmaria.fimia@inmi.it (G.M.F.)

degradation of the desmosome component plakoglobin (*19*). Studies on *Trim32* KO mice have shown that TRIM32 is not necessary to trigger muscle atrophy, but it plays a key role in muscle regrowth after atrophy (*20*). This finding is in agreement with the observation that patients with LGMD2H often manifest loss of motility after prolonged immobilization (*21*). Defective muscle regeneration was also observed in *Trim32* KO mice upon damage induced by cardiotoxin treatment (*22*). Muscle regrowth failure after atrophy has been ascribed to the impaired degradation of PIAS4, a SUMO (small ubiquitin-like modifier) ligase that induces premature senescence (*20*), and of the proliferation inhibitor NDRG2 (*23*). Whether TRIM32 also plays a protective role in differentiated muscle cells during or after atrophy induction remains to be elucidated.

Recently, several members of the TRIM protein family have been demonstrated to promote autophagy induction by interacting with the upstream regulators ULK1 (Unc-51 like autophagy activating kinase 1) and BECLIN 1 (*24*–*27*). In addition, TRIM proteins act as cargo receptors for selective autophagy (*27*–*29*).

AMBRA1 (activating molecule in BECN1-regulated autophagy protein 1) is a positive regulator of autophagy that binds and regulates BECLIN 1 and ULK1 activity (*30*–*33*) by favoring their non-degradative ubiquitination. In addition, AMBRA1 interacts with the E3 ubiquitin ligases CULLIN4 and CULLIN5 (*34*) to regulate the temporal dynamics of autophagy response and, with PARKIN and HUWE1, to promote mitophagy (*35*, *36*). Evidence of a role of AMBRA1 in muscle homeostasis have been recently reported (*37*). Ablation of AMBRA1 in zebrafish leads to a severe myopathy characterized by disorganized myofibers and aberrant mitochondria morphology (*37*). Abnormal muscle structure organization was also observed in AMBRA1 mutant mouse embryos (*37*). Here, we show that AMBRA1 interacts with TRIM32 and mediates autophagy induction in muscle cells under atrophic conditions by stimulating ULK1 activity via unanchored K63-linked polyubiquitin.

## RESULTS

### AMBRA1 interacts with the E3 ubiquitin ligase TRIM32

AMBRA1 was found in association with TRIM32 in a mass spectrometry–based protein interaction screening (*34*). The binding between AMBRA1 and TRIM32 was confirmed by coimmunoprecipitation in 293 T cells expressing MYC-AMBRA1 and FLAG-TRIM32 proteins (Fig. 1A) and in C2.7 myoblast cells at endogenous levels (Fig. 1B). The domains of AMBRA1 and TRIM32 responsible for their interaction were mapped by means of deletion mutants. Coimmunoprecipitation experiments in 293 T cells transfected with vectors encoding the N-terminal, central, or C-terminal region of AMBRA1 showed that TRIM32 preferentially associates with the C-terminal part of AMBRA1 (Fig. 1C). On the other hand, coimmunoprecipitation experiments in *TRIM32* KO 293 T cells transfected with TRIM32 mutants encoding the catalytic domain (RING/B-box), the coiled-coil domain, or the NHL repeats showed that the catalytic domain of TRIM32 is responsible for the binding to Ambra1 (Fig. 1D).

### TRIM32 is required for the induction of autophagy by atrophic stimuli

The interaction of TRIM32 with AMBRA1 prompted us to analyze the role of TRIM32 in the regulation of autophagy in muscle cells. We performed experiments in a murine myoblast cell line (C2.7 cells), which is able to differentiate into myotubes upon serum withdrawal. At first, we asked whether AMBRA1 and TRIM32 were required for sustaining basal autophagy in undifferentiated and differentiated cells. We measured autophagy flux in cells in which AMBRA1 or TRIM32 expression was down-regulated by using specific lentiviral short hairpin RNAs (shRNA; shAmbra1 and shTrim32). Analysis of LC3-II levels in the presence or absence of lysosome inhibitors revealed that basal autophagy flux is defective when AMBRA1 expression is silenced both in myoblasts and myotubes (fig. S1A). We also observed a partial inhibition of the myosin heavy chain expression, accordingly to the role of basal autophagy in supporting the differentiation of C2 myoblasts (*38*). In contrast, we observed no significant alterations of autophagy flux in either undifferentiated or differentiated cells in which TRIM32 expression was down-regulated, indicating that TRIM32 is dispensable for sustaining basal autophagy (fig. S1B).

TRIM32 was reported to play an important role in muscle fiber recovery from atrophic conditions (*20*). Since autophagy is up-regulated during muscle atrophy (*5*), we decided to investigate the role of TRIM32 in the induction of autophagy in response to atrophic stimuli. To set up the experimental conditions to induce muscle atrophy in vitro, we treated the differentiated C2.7 cells with dexamethasone, a synthetic analog of glucocorticoids, for 24 hours and verified atrophy induction by analyzing the expression level of the atrophic gene *MuRF1* (fig. S2A). In parallel, we evaluated autophagy flux after 4 hours of treatment by LC3 immunoblotting analysis, which confirmed that autophagy is induced by dexamethasone (fig. S2B).

Similar to that observed in basal autophagy, shAmbra1 C2.7 cells treated with dexamethasone showed lower LC3-II levels (fig. S2C). Notably, a significant impairment of autophagy induction was also observed when TRIM32 knock-down or KO myotubes were exposed to dexamethasone (Fig. 2A and fig. S2, D and E). Autophagy impairment upon TRIM32 down-regulation was not restricted to C2.7 cells, as a similar defect was also observed in rat L6E9 myoblasts upon dexamethasone treatment (fig. S2F). We confirmed failure of Trim32-silenced C2.7 cells to increase autophagy flux by measuring the lysosomal degradation rate of the autophagy cargo receptor NBR1(next to BRCA1 gene 1 protein) at a later time point of dexamethasone treatment (fig. S3A), as well as by ultrastructural analysis. In particular, transmission electron microscopy showed that the number of degradative compartments (amphisomes, lysosomes, and autolysosomes) per cell section, which reflects autophagic activity (*39*), was similar in untreated shControl and shTrim32 C2.7 cells (fig. S3B), corroborating that TRIM32 is not involved in basal autophagy. Atrophy stimulation in control cells led to an increased number of degradative compartments per cell section, confirming autophagy induction under these conditions (Fig. 2B and fig. S3C, top). In contrast, no increase was observed in TRIM32-depleted cells exposed to dexamethasone, underlying that TRIM32 is required for autophagy in atrophic myotubes (Fig. 2B and fig. S3C, bottom).

To substantiate the involvement of TRIM32 in the regulation of autophagy in atrophic conditions, we analyzed autophagy flux upon nutrient deprivation as an alternative atrophic stimulus. Also, in this case, a reduced induction of autophagy was observed in TRIM32-silenced cells when LC3-II levels were analyzed (fig. S4A). We confirmed defective autophagy by measuring the lysosomal degradation rate of the autophagy cargo receptor p62 in shTrim32-silenced cells at a later time point of nutrient deprivation (fig. S4B).

We then assessed whether TRIM32 is required for an efficient autophagy response to atrophic stimuli in vivo using a mouse model of *Trim32* deficiency (*22*). We treated *Trim32* wild-type (WT) and

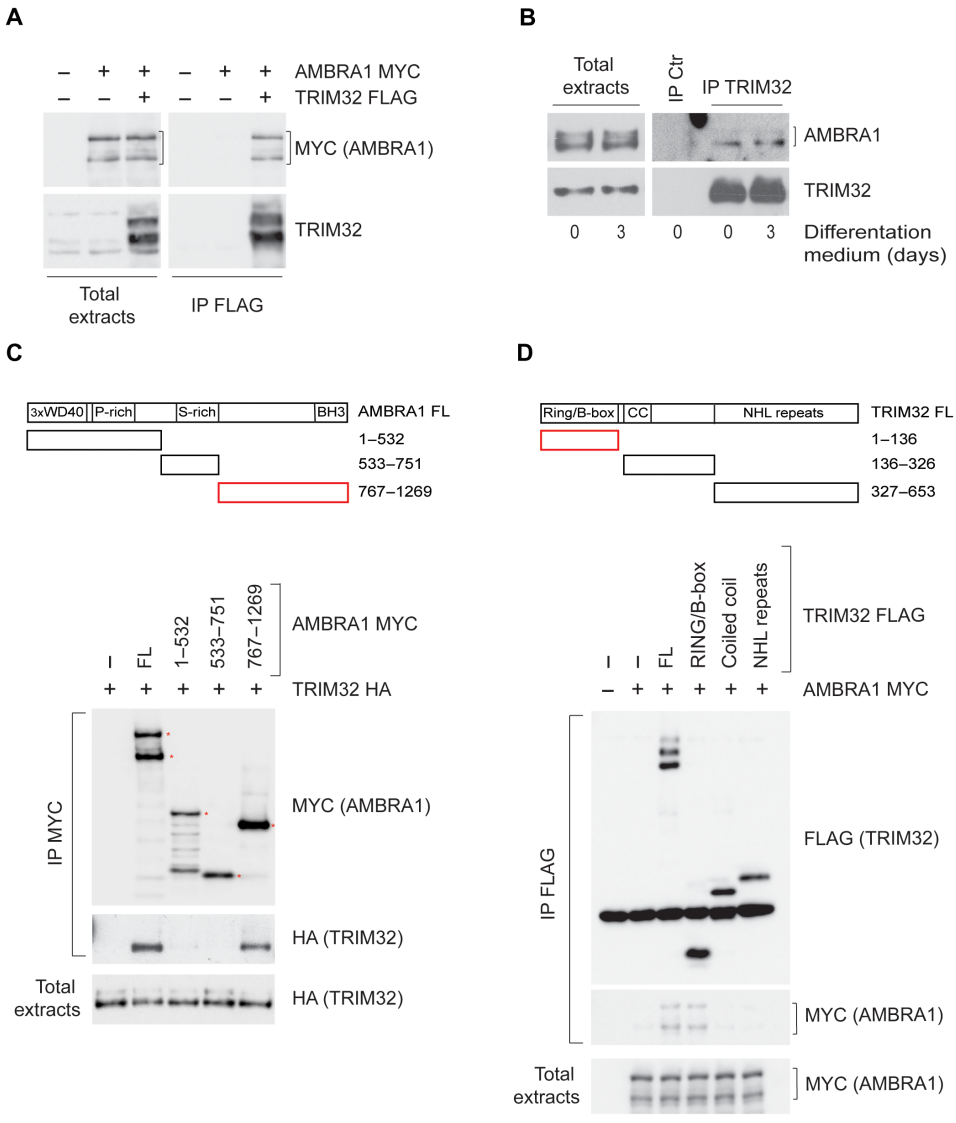


**Fig. 1. TRIM32 binds to AMBRA1.** (**A**) Protein extracts from MYC-AMBRA1– and FLAG-TRIM32–transfected 293 T cells were subjected to immunoprecipitation (IP) using an anti-FLAG antibody. Immunopurified complexes were analyzed by immunoblotting using anti-MYC and anti-TRIM32 antibodies. (**B**) Undifferentiated and differentiated C2.7 cells were lysed, and protein extracts were immunoprecipitated using an anti-TRIM32 antibody. An unrelated antibody was used as a negative control (IP Ctr). Immunopurified complexes were analyzed by immunoblotting using anti-AMBRA1 and anti-TRIM32 antibodies. (**C**) 293 T cells were cotransfected with vectors encoding HA-TRIM32 and the following MYC-AMBRA1 constructs: full length (FL), N-terminal (amino acids 1 to 532), central (amino acids 533 to 751), and C-terminal region (amino acids 767 to 1269). Protein extracts were immunoprecipitated using an anti-MYC antibody. Immunopurified complexes were analyzed by immunoblotting using anti-HA and anti-MYC antibodies. A scheme of the AMBRA1 domain architecture is shown (P-rich, proline-rich domain; S-rich, serine-rich domain; BH3, Bcl2 homology 3 domain). The red bar indicates the TRIM32-interacting domain. Asterisks indicate bands of AMBRA1 at the expected molecular weights. (**D**) *TRIM32* KO 293 T cells were cotransfected with vectors encoding MYC-AMBRA1 and the following FLAG-TRIM32 constructs: full length, catalytic domain (RING/B-box, amino acids 1 to 136), central region containing the coiled-coil domain (amino acids 136 to 326), and NHL repeats (amino acid 327 to 653). Protein extracts were immunoprecipitated using anti-FLAG antibody. Immunopurified complexes were analyzed by immunoblotting using anti-FLAG and anti-MYC antibodies. A scheme of the TRIM32 domain architecture is shown (CC, coiled-coil domain). The red bar indicates the AMBRA1-interacting domain.

KO mice with dexamethasone for 8 hours and analyzed LC3, NBR1, and p62 levels in quadricep muscles by immunoblotting. As shown in Fig. 2C, a significant impairment of autophagy is observed in *Trim32* KO mice upon dexamethasone treatment when compared to the WT counterpart. NBR1 and p62 RNA levels were also measured by quantitative polymerase chain reaction (qPCR) to rule out a transcriptional contribution to the observed changes (fig. S5, A and B). Defective autophagy response was confirmed by confocal microscopy as well. Quadricep muscles from WT mice treated with dexamethasone showed a robust increase of LC3-positive vesicles, which mostly colocalize with the cargo receptor p62 (fig. S5, C and D). Instead, the accumulation of LC3-positive vesicles was reduced

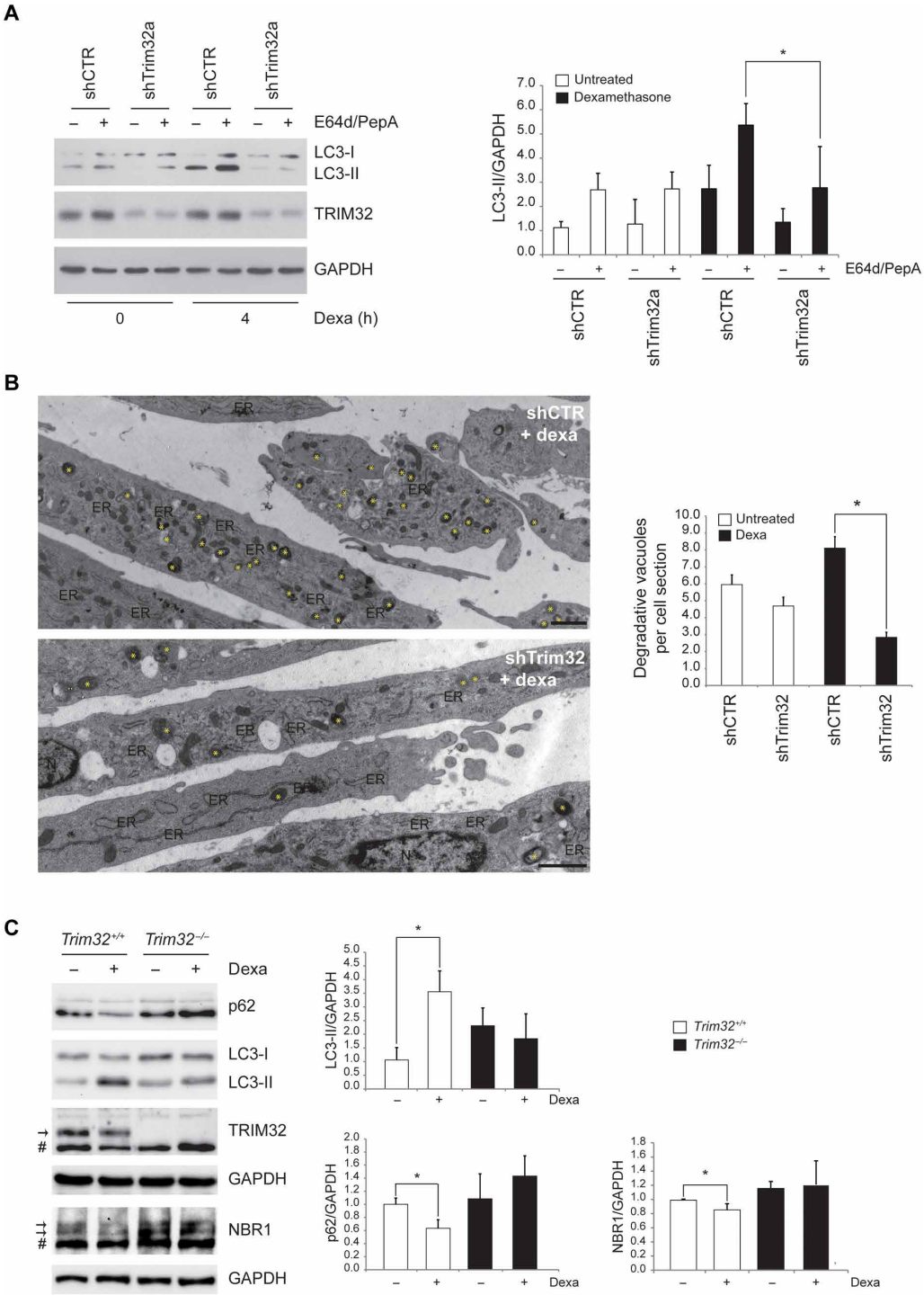


**Fig. 2. Trim32 is required for autophagy induction by atrophic stimuli in muscle cells.** (**A**) shCTR and shTrim32 C2.7 cells differentiated for 3 days were treated with dexamethasone (dexa) for 4 hours (h) or left untreated. One hour before lysis, cells were incubated with the lysosome inhibitors E64d and pepstatin A (E64d/PepA), as indicated. LC3-II and TRIM32 levels were analyzed by immunoblotting (left). GAPDH (glyceraldehyde-3-phosphate dehydrogenase) was included as a loading control. The graph (right) reports means ± SD of LC3-II/GAPDH values from three independent experiments; *$P < 0.05$. (**B**) Differentiated shCTR and shTrim32 C2.7 cells were treated with dexamethasone for 4 hours and processed for EM. ER, endoplasmic reticulum; N, nucleus. Yellow asterisks highlight degradative compartments (amphisomes, lysosomes, and autolysosomes). Scale bars, 1 μm. The graph (right) reports means ± SEM of degradative vacuoles per cell per section. Images of untreated cells are reported in fig. S3B. (**C**) WT (*Trim32*$^{+/+}$) and KO (*Trim32*$^{-/-}$) mice were injected with dexamethasone (5 mg/kg) or saline solution (0.9% NaCl) as a negative control. Mice were sacrificed 8 hours after injection, and protein extracts were prepared from quadricep muscles. LC3-II, NBR1, and p62 levels were analyzed by immunoblotting (left). Arrows point to TRIM32- and NBR1-specific bands; the number sign (#) indicates nonspecific signals. The graph (right) reports means ± SD of LC3-II/GAPDH, NBR1/GAPDH, and p62/GAPDH values from at least three independent experiments; *$P < 0.05$.

in Trim32 KO mice with the residual ones, showing diminished colocalization with p62 (fig. S5, E and F).

Autophagy inhibition is known to exacerbate muscle damage in response to atrophic stimuli, resulting in the accumulation of reactive oxygen species (ROS) from dysfunctional mitochondria and an increased induction of atrophic genes (*40*, *41*). Therefore, we assessed whether these alterations were associated with the autophagy impairment observed upon TRIM32 inhibition. TRIM32-silenced myotubes and the relative controls were treated with dexamethasone, and the production of ROS was analyzed after 24 hours (fig. S6A), while the expression of the atrophic gene MuRF1 was monitored at 8 and 24 hours (fig. S6, B and C). We also treated control cells with the autophagy inhibitor 3-methyladenine (3MA), as a positive control of autophagy inhibition (fig. S6D). Concomitantly, we analyzed LC3-II levels at 24 hours after dexamethasone treatment to confirm that autophagy impairment was still present at the time points where ROS and MuRF1 levels were measured (fig. S6E). Results showed that both atrophy-related parameters were worsened in TRIM32-silenced cells, similar to those observed in control cells exposed to 3MA. Together, these results point to a role of TRIM32 in the regulation of autophagy in atrophic conditions.

### TRIM32 stimulates ULK1 activity in an AMBRA1-dependent manner through unanchored K63-linked polyubiquitin

TRIM proteins were reported to control autophagy by modulating the activity of BECLIN 1 and ULK1 (*27*). We therefore asked whether TRIM32 could regulate autophagy by interacting with these autophagy regulators. Coimmunoprecipitation experiments performed in 293 T cells transfected with vectors encoding TRIM32, ULK1, and BECLIN 1 showed that TRIM32 efficiently interacts with ULK1 (Fig. 3A). This interaction is specific for ULK1, since the binding with BECLIN 1 was not observed in the same experimental settings (Fig. 3A). We mapped the domain of TRIM32 responsible for ULK1 interaction by immunoprecipitation of a series of TRIM32 deletion mutants, which showed that TRIM32 binds ULK1 through its catalytic domain (Fig. 3B). On the basis of the ability of AMBRA1 to associate with both ULK1 and TRIM32, we asked whether AMBRA1 plays a role in the interaction between these proteins. Coimmunoprecipitation analysis showed that the association between TRIM32 and ULK1 is strongly affected when AMBRA1 expression is down-regulated (Fig. 3C), indicating that AMBRA1 is required to assemble TRIM32 and ULK1 in a complex.

Since TRIM32 is an E3 ubiquitin ligase, we assessed whether its interaction with ULK1 results in an increase of ULK1 ubiquitination. To this aim, we analyzed degradative and nondegradative ubiquitination of endogenous ULK1 in TRIM32-transfected 293 T cells using K48- and K63-linked polyubiquitin chain antibodies, respectively. As shown in Fig. 4A, TRIM32 triggers K63-linked ubiquitination of ULK1, while K48-linked ubiquitination remains unaltered (fig. S7A). The increase in ULK1 ubiquitination depends on the ligase activity of TRIM32, since a catalytic-inactive mutant is not able to trigger ULK1 ubiquitination (fig. S7B). We also confirmed the ability of TRIM32 to ubiquitinate ULK1 by in vitro assays using either recombinant or immunopurified ULK1 (Fig. 4B and fig. S7C). In keeping with its role in TRIM32-ULK1 complex formation, AMBRA1 down-regulation leads to a significant decrease of TRIM32-mediated ubiquitination of ULK1 (Fig. 4C).

Since TRIM32 was reported to produce both substrate-linked and free polyubiquitin chains (*23*, *42*), we analyzed whether TRIM32-induced modification of ULK1 is due to either covalent ubiquitination or

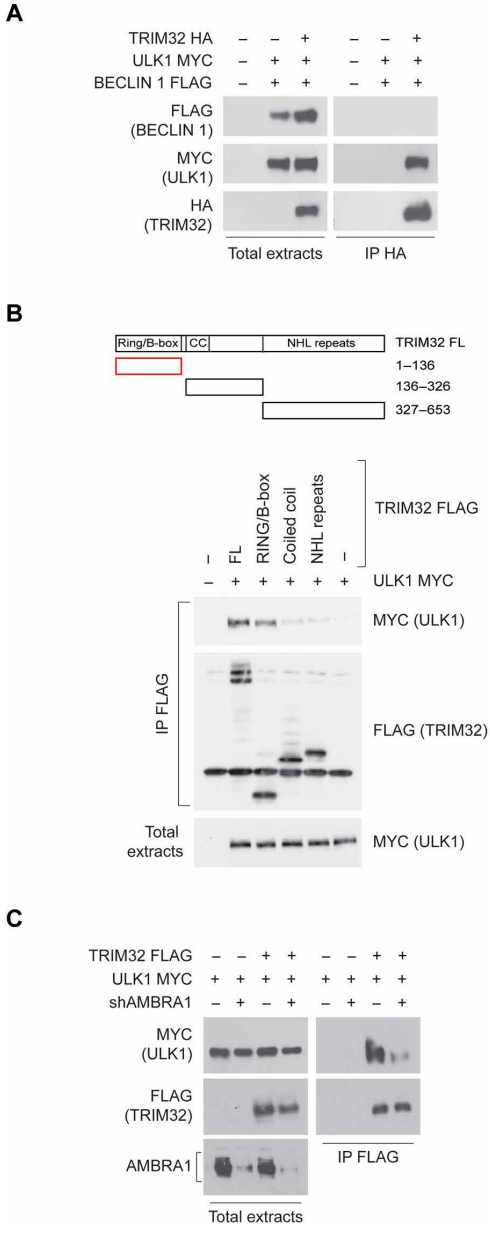


**Fig. 3. TRIM32 associates with ULK1 in an AMBRA1-dependent manner.** (**A**) Protein extracts from 293 T cells transfected with vectors encoding HA-TRIM32, FLAG–BECLIN 1, and MYC-ULK1, as indicated, were subjected to immunoprecipitation using an anti-HA antibody. Immunopurified complexes were analyzed by immunoblotting using anti-FLAG, anti-MYC, and anti-HA antibodies. (**B**) *TRIM32* KO 293 T cells were cotransfected with vectors encoding MYC-ULK1 and the following FLAG-TRIM32 constructs: full length, catalytic domain (RING/B-box, amino acids 1 to 133), central region containing the coiled-coil domain (amino acids 134 to 198), and NHL repeats (amino acids 199 to 325). Protein extracts were immunoprecipitated using an anti-FLAG antibody. Immunopurified complexes were analyzed by immunoblotting using anti-FLAG and anti-MYC antibodies. A scheme of the TRIM32 domain architecture is shown; the red bar indicates the ULK1-interacting domain. (**C**) Control shRNA and shAmbra1 293 T cells were transfected with a vector encoding MYC-ULK1, alone or in combination with FLAG-TRIM32. Cells were lysed, and protein extracts were subjected to immunoprecipitation using an anti-FLAG antibody. Immunopurified complexes were analyzed by immunoblotting using anti-MYC and anti-FLAG antibodies. Total extracts were also probed with an anti-AMBRA1 antibody to verify AMBRA1 silencing.

the binding to unanchored polyubiquitin. To this aim, we subjected ubiquitinated ULK1, immunopurified from either TRIM32-transfected cells or an in vitro assay, to heat denaturation to disrupt noncovalent interactions. Immunoblotting analysis showed that the ubiquitination signal is lost following denaturation [Fig. 4, B and D (see lanes labeled as Re-IP)], indicating that ULK1 binds noncovalently to K63-linked polyubiquitin chains produced by TRIM32. Moreover, we observed that the interaction with the polyubiquitin chains is mediated by the C-terminal domain of ULK1, as shown by cotransfecting TRIM32 with ULK1 deletion mutants (fig. S7D).

Since K63-linked ubiquitination of ULK1 stimulates its kinase activity (*31*), we asked whether TRIM32 is able to promote ULK1 proautophagic function. A phosphorylation analysis of the autophagic proteins VPS34 and BECLIN 1, two well-characterized targets of ULK1 (*43*, *44*), showed that ULK1 kinase activity is potentiated by TRIM32 (Fig. 4, E and F). In line with these results, we also observed that overexpression of WT TRIM32, but not of the catalytic mutant C39S, results in an increased autophagy flux, as revealed by LC3 immunoblotting (fig. S7E). Together, these data indicate that TRIM32 can induce autophagy by interacting with ULK1 in an AMBRA1-dependent manner and promoting its activity through unanchored polyubiquitin.

### TRIM32 is required for ULK1 activation through K63-linked polyubiquitin in atrophic conditions

The ability of TRIM32 to bind and activate ULK1 through unanchored polyubiquitin prompted us to analyze the functional relation between TRIM32 and ULK1 in the induction of autophagy by atrophic stimuli. First, by coimmunoprecipitation assays performed in untreated and dexamethasone-treated C2.7 cells, we observed that atrophy induction stimulates the interaction of ULK1 with TRIM32 (Fig. 5A), as well as its association with K63-linked polyubiquitin (Fig. 5B). Then, we investigated whether TRIM32 is required for the increased association of ULK1 to K63-linked polyubiquitin upon atrophy stimulation. Down-regulation of TRIM32 expression in C2.7 cells by RNA interference markedly reduced the amount of K63-linked polyubiquitin that coimmunoprecipitated with ULK1 upon dexamethasone treatment (Fig. 5C). Consistently, ULK1 activity was decreased upon TRIM32 down-regulation, as shown by analyzing the phosphorylation status of BECLIN 1 and ATG14 (AuTophaGy related 14), two ULK1 substrates (Fig. 5, D and E). Together, these results indicate that autophagy impairment in TRIM32-deficient muscle cells is associated with a defective activation of ULK1 mediated by K63-linked polyubiquitin.

We also confirmed the key role of ULK1 in the response to atrophic stimuli by inhibiting the expression of NEDD4L, an E3 ubiquitin ligase that targets ULK1 to proteasome-mediated degradation (*45*). As shown in fig. S8 (A and B), NEDD4L silencing in C2.7 myoblasts resulted in ULK1 protein stabilization, leading to a higher autophagy induction by nutrient starvation.

### TRIM32 pathogenic mutants are defective for ULK1 binding and autophagy induction

Specific mutations in *TRIM32* are causative of the muscular disease LGMD2H (*12*). Since autophagy dysregulation plays an important role in various muscular dystrophies (*4*), we asked whether the disease-associated TRIM32 mutants have an impaired proautophagic activity. First, TRIM32 mutants were tested for the ability to bind ULK1 in a coimmunoprecipitation experiment. As shown in Fig. 6A, the binding of TRIM32 to ULK1 is severely affected by all tested pathogenic mutations. Since the ULK1-interacting domain of TRIM32 is different from the NHL repeats (see Fig. 3B), where the disease-associated mutations are located, we decided to better elucidate the role of this domain in the binding to ULK1 by generating a TRIM32 mutant lacking the entire NHL repeats. When tested in a coimmunoprecipitation assay, the ΔNHL TRIM32 mutant also failed to interact with ULK1 (fig. S8C), indicating that, although not sufficient for the binding, the NHL repeats need to be present to allow the interaction of TRIM32 with ULK1 in the context of the entire protein.

We also tested whether pathogenic mutations affect the interaction between TRIM32 and AMBRA1. We observed that AMBRA1 is still able to interact with all mutants tested, suggesting that pathogenic mutations specifically impair the interaction with ULK1 (fig. S8D).

To verify whether the defective binding of Trim32 pathogenic mutants with ULK1 affects their ability to stimulate ULK1 proautophagic activity, we further characterized two of them: $Trim32^{D487N}$ and $Trim32^{R394H}$. First, we analyzed the levels of ULK1-associated polyubiquitin and of ULK1-mediated BECLIN 1 phosphorylation upon TRIM32 WT or mutant protein overexpression in 293 T cells. We found that both pathogenic TRIM32 mutants showed a reduced ability to promote ULK1 association to K63-linked polyubiquitin (fig. S8E) and BECLIN 1 phosphorylation on $Ser^{15}$ (fig. S8F), confirming their defective ability to induce ULK1 activity.

Then, we analyzed whether the pathogenic TRIM32 mutants have an impaired ability to induce autophagy in response to atrophy induction in myobast cells. To this aim, we complemented *Trim32* KO C2.7 cells with retroviral vectors expressing TRIM32 WT, pathogenic mutants $Trim32^{D487N}$ and $Trim32^{R394H}$, or the catalytic mutant $Trim32^{C39S}$. We treated cells with dexamethasone and analyzed autophagy flux by measuring LC3-II (Fig. 6B and fig. S9, A and B) and NBR1 (fig. S9C) levels in the presence or absence of lysosome inhibitors. Immunoblot analysis showed that TRIM32 mutants have an impaired autophagic induction. Also, in this case, the inability of TRIM32 mutants to trigger autophagy was associated with a defective activity of ULK1, as shown by analyzing phosphorylation of BECLIN 1 and ATG14 on $Ser^{15}$ and $Ser^{29}$, respectively (fig. S10, A and B).

Last, we evaluated whether cells obtained from a patient with LGMD2H show a defective autophagy response to dexamethasone-induced atrophy. To this aim, fibroblasts from a healthy donor (HD) and a patient with LGMD2H, carrying a complete gene deletion in one allele and a nonsense c.1837 C > T (R613X) mutation in the NHL domain of the other allele (*46*), were transdifferentiated in myoblasts by MYOD ectopic expression (fig. S10C). We treated cells with dexamethasone and analyzed LC3-II levels in the presence or absence of lysosome inhibitors to measure autophagic flux. Notably, autophagy induction by dexamethasone treatment was impaired in myotube cells carrying a *TRIM32* mutation (Fig. 6C and fig. S10D). Moreover, in line with that observed in Trim32-silenced cells, atrophy induction was exacerbated in LGMD2H patient cells, as indicated by analyzing MuRF1 levels (fig. S10E). Together, these results show that disease-associated mutations affect the proautophagic function of TRIM32 (fig. S10F).

## DISCUSSION

Autophagy is critical for muscle adaptation to sublethal cellular stress (*47*). Exercise increases autophagy levels to meet energetic demands and to eliminate dysfunctional cell constituents, such as mitochondria and sarcomere proteins, which may accumulate during contraction

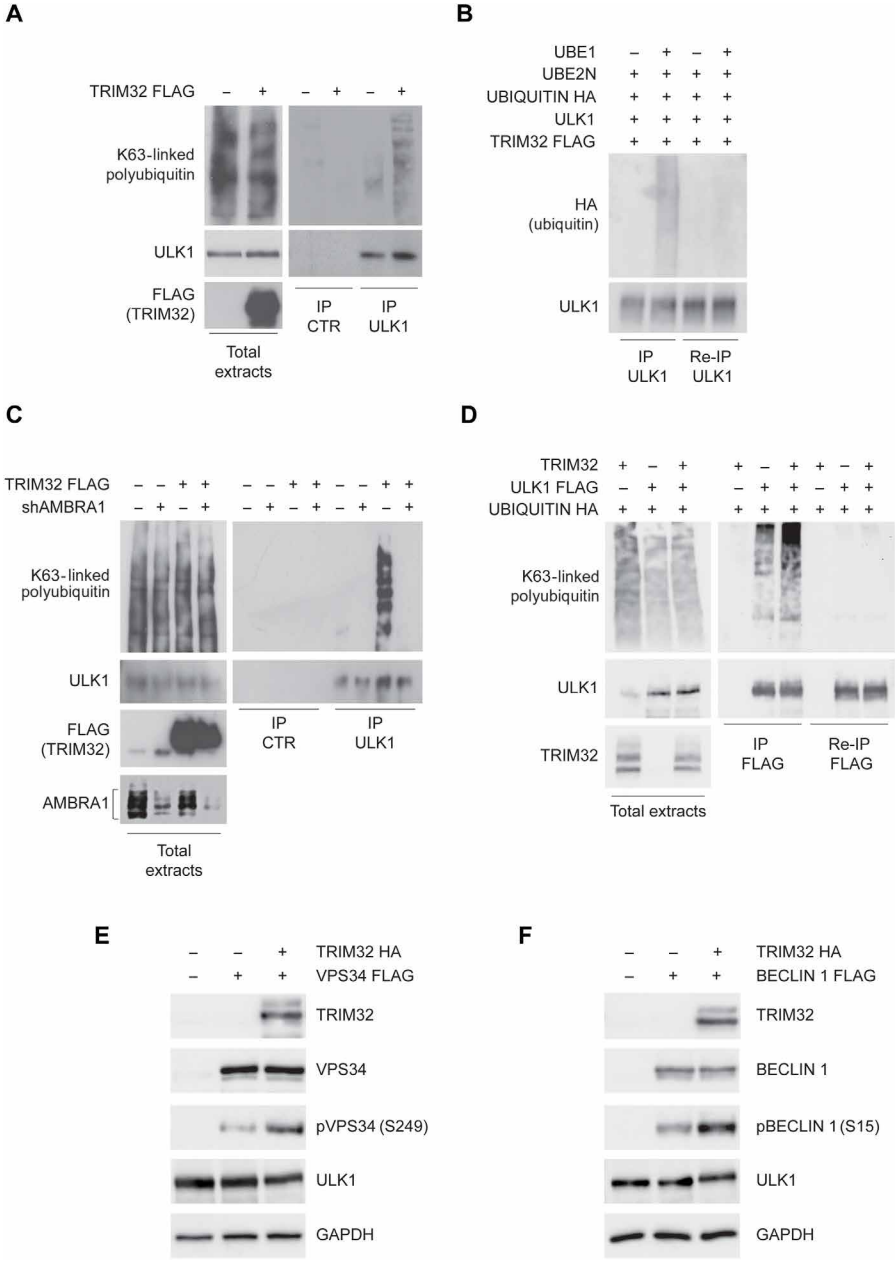


**Fig. 4. TRIM32 stimulates ULK1 activity in an AMBRA1-dependent manner through unanchored K63-linked polyubiquitin.** (**A**) Protein extracts from FLAG-TRIM32–transfected 293 T cells were subjected to immunoprecipitation using an anti-ULK1 antibody. Immunopurified complexes were analyzed by immunoblotting to detect ULK1 and K63-linked ubiquitin. Total extracts were also probed with an anti-FLAG antibody to verify TRIM32 transfection. (**B**) In vitro ULK1 ubiquitination assay using immunopurified Flag TRIM32 and recombinant ULK1, HA ubiquitin, E1 Ub–activating enzyme (UBE1), and E2 Ub–conjugating enzyme (UBE2N). Reactions were also performed in the absence of UBE1 to verify ubiquitination reaction specificity. At the end of the reaction, ULK1 was immunopurified and ubiquitination evaluated by immunoblotting using an anti-HA antibody (lanes 1 and 2). To verify whether ubiquitin was covalently linked, immunopurified ULK1 was boiled in 1% SDS after the ubiquitination reaction, reimmunoprecipitated (Re-IP), and analyzed by immunoblotting using anti-HA and anti-ULK1 antibodies (lanes 3 and 4). (**C**) shCtr or shAmbra1 293 T cells were transfected with a vector encoding FLAG-TRIM32 or an empty vector (–). Protein extracts were immunoprecipitated using an anti-ULK1 antibody. Immunopurified complexes were analyzed by immunoblotting to detect ULK1 and K63-linked ubiquitin. Total extracts were also probed with FLAG and AMBRA1 antibodies to verify TRIM32 transfection and AMBRA1 silencing, respectively. (**D**) 293 T cells were transfected with vectors encoding HA-tagged ubiquitin, FLAG-ULK1, and TRIM32, as indicated. Protein extracts were subjected to immunoprecipitation using an anti-FLAG antibody. Immunopurified complexes were analyzed by immunoblotting to detect K63-linked ubiquitin and ULK1 using specific antibodies. TRIM32 expression was also analyzed in total extracts. To verify whether ubiquitin was covalently linked, immunopurified FLAG-ULK1 was boiled in 1% SDS, reimmunoprecipitated, and analyzed by immunoblotting using anti–K63-linked ubiquitin and anti-ULK1 antibodies. (**E**) 293 T cells were transfected with vectors encoding FLAG-VPS34, alone or in combination with HA-TRIM32. TRIM32, VPS34, and phospho-VSP34 [pVPS34; $Ser^{249}$ (S249)] were analyzed by immunoblotting. GAPDH was included as a loading control. (**F**) 293 T cells were transfected with vectors encoding FLAG–BECLIN 1, alone or in combination with HA-TRIM32. The levels of TRIM32, BECLIN 1, and phospho–BECLIN 1 [pBECLIN 1; $Ser^{15}$ (S15)] were analyzed by immunoblotting. GAPDH was included as a loading control.

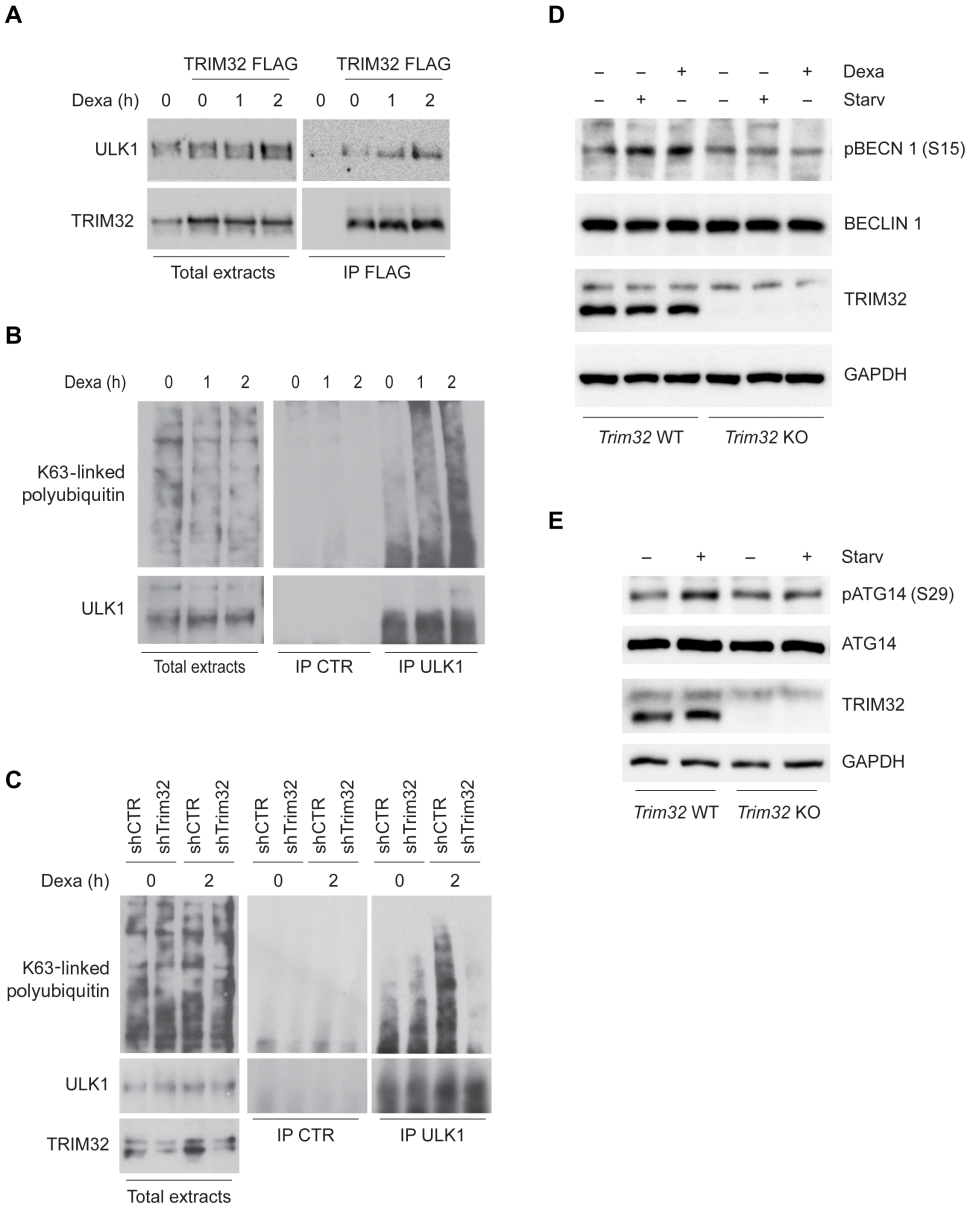


**Fig. 5. TRIM32 is required for ULK1 activation through K63-linked polyubiquitin upon dexamethasone treatment.** (**A**) FLAG-TRIM32–expressing C2.7 cells differentiated for 3 days were treated with dexamethasone for 1 and 2 hours. Protein extracts were immunoprecipitated using an anti-FLAG antibody. Immunopurified complexes were analyzed by immunoblotting to detect the presence of TRIM32 and ULK1 using specific antibodies. (**B**) C2.7 cells differentiated for 3 days were treated with dexamethasone for 1 and 2 hours. Protein extracts were immunoprecipitated using an anti-ULK1 antibody. Immunopurified complexes were analyzed by immunoblotting to detect the presence of ULK1 and K63-linked polyubiquitin. An unrelated antibody was used as a negative control (IP CTR). (**C**) shCTR and shTrim32 C2.7 cells differentiated for 3 days were treated with dexamethasone for 2 hours. Protein extracts were immunoprecipitated using an anti-ULK1 antibody. Immunopurified complexes were analyzed by immunoblotting to detect the presence of ULK1 and K63-linked ubiquitin. An unrelated antibody was used as a negative control. Total extracts were probed with an anti-TRIM32 antibody to verify silencing efficiency. (**D**) BECLIN 1 overexpressing *Trim32* WT and KO C2.7 cells were differentiated for 3 days and incubated with dexamethasone or nutrient-deprived medium (Starv) for 2 hours. Protein extracts were analyzed by immunoblotting to measure the levels of phospho–BECLIN 1 [pBCN 1 ($Ser^{15}$)], BECLIN 1, and TRIM32. GAPDH was included as a loading control. (**E**) *Trim32* WT and KO C2.7 cells differentiated for 3 days were incubated with dexamethasone for 2 hours. Cells were lysed, and protein extracts were analyzed by immunoblotting to measure the levels of phospho-ATG14 [pATG14 ($Ser^{29}$)], ATG14, and TRIM32. GAPDH was included as a loading control.

(*48*, *49*). Autophagy is also induced during prolonged inactivity or other atrophic stimuli, mainly to ensure the removal of surplus of organelles, such as mitochondria and sarcoplasmic reticulum, during muscle fiber remodeling (*50*). Although it contributes to muscle dismantling, autophagy is considered a protective mechanism by preventing the accumulation of harmful signals, such as ROS, generated by inoperative compartments (*4*).

How autophagy is regulated in muscle cells has been extensively investigated at a transcriptional level, highlighting the important role of FoxO, glucocorticoid receptors, nuclear factor κB (NF-κB),

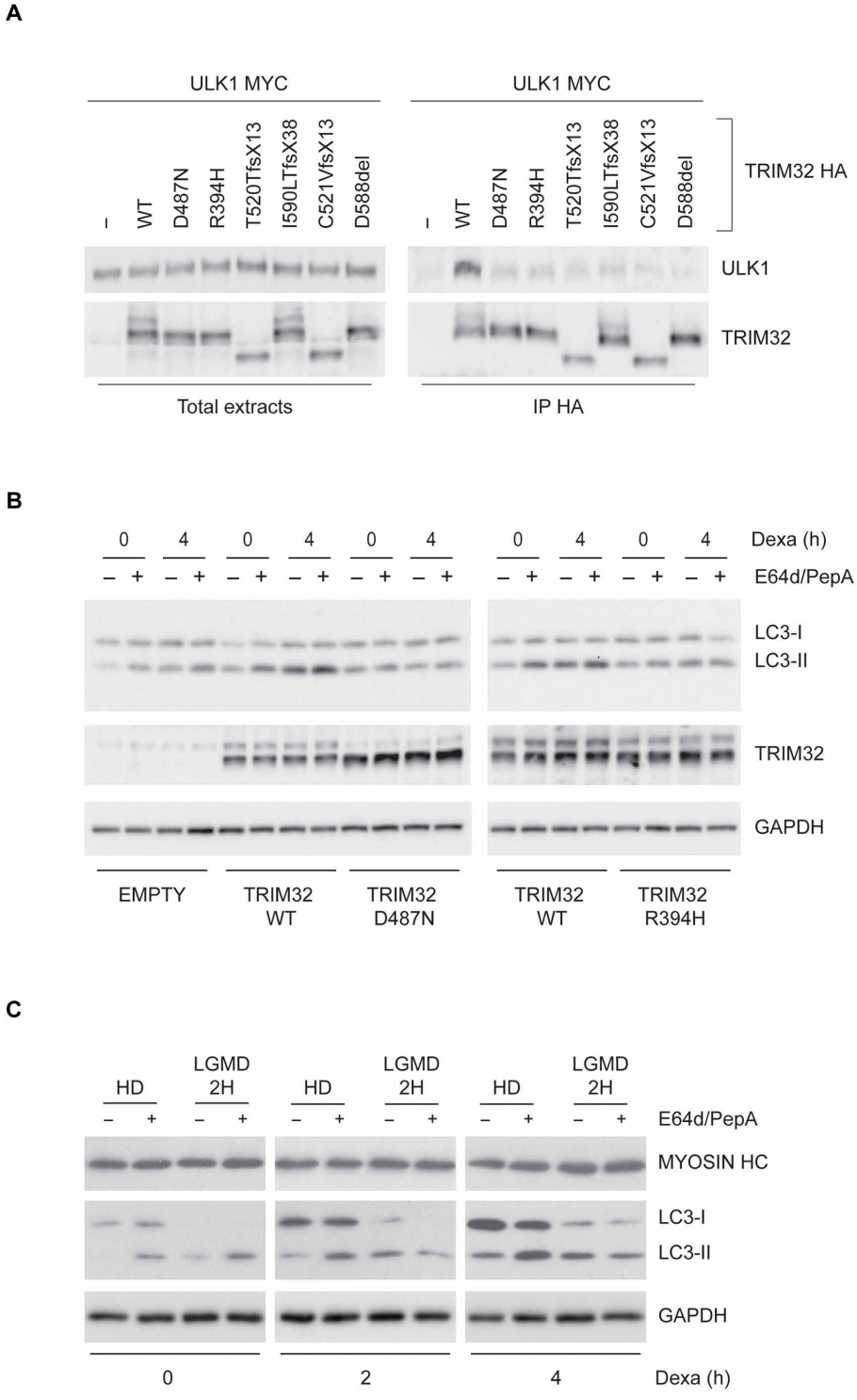


**Fig. 6. TRIM32 pathological mutants are unable to interact with ULK1 and promote autophagy.** (**A**) 293 T cells were transfected with a vector encoding for MYC-ULK1, alone or in combination with HA-TRIM32 WT, or the indicated pathogenic TRIM32 mutants. Protein extracts were subjected to immunoprecipitation using an anti-HA antibody. Immunopurified complexes were analyzed by immunoblotting to detect the presence of TRIM32 and ULK1. (**B**) *TRIM32* KO C2.7 cells were infected with retroviruses encoding WT FLAG-TRIM32 or the indicated pathogenic TRIM32 mutants. EMPTY, *TRIM32* KO C2.7 cells infected with noncoding retroviruses. Upon 3 days in differentiation medium, cells were treated with dexamethasone for 4 hours and incubated with the lysosome inhibitors E64d and pepstatin A for 1 hour before lysis, as indicated. LC3-II and TRIM32 levels were analyzed by immunoblotting using specific antibodies. GAPDH was included as a loading control. (**C**) Fibroblasts from a WT donor and a patient with LGMD2H were transdifferentiated to myoblasts by MYOD (myogenic differentiation 1) ectopic expression. Cells differentiated for 3 days were treated, or not, with dexamethasone for 2 and 4 hours. One hour before lysis, cells were incubated with the lysosome inhibitors E64d and pepstatin A, as indicated. LC3-II and myosin heavy chain (MYOSIN HC) levels were analyzed by immunoblotting (bottom panel). GAPDH was included as a loading control.

and SMAD transcription factors (*51*). In contrast, the mechanisms by which stresses related to muscle inactivity are transduced to the autophagy machinery for the activation of the process remain less characterized.

Here, we report that the E3 ubiquitin ligase TRIM32 is required for the induction of autophagy in muscle cells by atrophic stimuli using both in vitro and in vivo models. The proautophagic activity of TRIM32 resides in its ability to bind to AMBRA1 and ULK1 and to synthesize K63-linked polyubiquitin chains that bind noncovalently to ULK1 to promote its activity (fig. S10F).

Unanchored polyubiquitin chains are known to play a key role in the regulation of kinase activity (*52*). Most evidence come from studies on innate immune pathways, showing that transforming growth factor β–activated kinase 1 (TAK 1), inhibitor of nuclear factor κB kinase ε (IKKε), and NF-kappa-B essential modulator (NEMO) can be activated by the noncovalent interaction with polyubiquitin chains, which result in changes of the structural conformation and/or the interaction partners of these kinases (*53*–*55*). In this context, TRIM E3 ligases are emerging as key players (*56*), as shown for TRIM5, TRIM6, TRIM25, and TRIM32, with the latter adopting this strategy to activate NEMO in response to cytosolic double-stranded DNA (*42*). Here, we show that the unanchored polyubiquitin chains are also involved in the regulation of the autophagic process. TRIM32 synthesized K63-linked ubiquitin chains associated with ULK1 via its C-terminal domain, resulting in an augmented phosphorylation of its substrates BECLIN 1 and VPS34. In contrast to that reported for other TRIMs, we did not observe an increased interaction between ULK1 and BECLIN 1 complexes upon TRIM32 activation, suggesting that the binding with the polyubiquitin chains stimulates ULK1 activity rather than favoring protein complex interactions.

Our data also highlighted the central role of AMBRA1 in conveying multiple ubiquitin signals to the autophagy machinery for its activation in specific cellular contexts. In atrophic muscle cells, AMBRA1 acts as an essential cofactor, being required for both the interaction and the ubiquitination of ULK1 by TRIM32. AMBRA1 was previously shown to regulate ULK1 activity by mediating its covalent ubiquitination by the E3 ligase TNF receptor associated factor 6 (TRAF6) (*31*). Although the function of TRAF6 and TRIM32 may appear redundant in autophagy regulation, these proteins play opposite roles in the activation of the atrophy program (*20*, *57*, *58*). TRAF6 inactivation significantly impairs the induction of MuRF expression under atrophic conditions due to its role in the activation of the NF-κB pathway (*57*). Conversely, TRIM32 down-regulation leads to higher MuRF1 induction in myoblasts treated with dexamethasone, consistent with that observed when autophagy genes are deleted (*40*).

An important role of TRIM32 in muscle atrophy has been attributed to its ability to inhibit premature senesce of satellite cells responsible for muscle regrowth in vivo (*20*). Our results showing a defective muscle autophagy in atrophic conditions suggest that, in addition to regulating stem cells, TRIM32 may also contribute to the preservation of the function of differentiated muscle cells by reducing ROS accumulation and MuRF1 expression.

Evidence that the alteration of TRIM32-dependent autophagy may have an important implication in LGDM2H is underlined by two sets of data. First, we detected defective autophagy in myoblasts derived from fibroblasts of a patient with LGDM2H. Second, we found that disease-associated mutants of TRIM32 are unable to interact with ULK1 (their binding to AMBRA1, however, is unaffected) and to induce autophagy in muscle cells upon dexamethasone treatment, which is accompanied with accumulation of the autophagy cargo receptors NBR1 and p62, higher induction of MuRF1, and increased ROS production (fig. S10F). Further studies are required to clarify the molecular basis of this alteration, since the NHL repeats, where pathological mutations are located, do not mediate the interaction of TRIM32 with ULK1, which occurs through the RING/B-box region. We found that a TRIM32 mutant lacking the NHL repeats is also unable to bind ULK1, suggesting that this domain is essential to making the RING/B-box domain accessible to the targets in the presence of the coiled-coil region.

In conclusion, we have identified TRIM32 as an E3 ubiquitin ligase that regulates ULK1 activity in muscles under atrophy conditions, highlighting a novel autophagy pathway with potential relevance in human disorders. In light of these results, it is predictable that the proautophagic activity of TRIM32 could be relevant in other TRIM32-regulated processes, such as neuronal development, tumorigenesis, and immune response (*16*), in which its partner AMBRA1 is also playing important roles (*30*, *59*, *60*).

## MATERIALS AND METHODS

### Cell culture

293 T cells (American Type Culture Collection) were cultured in Dulbecco's modified Eagle's medium (DMEM) (Sigma-Aldrich, D6546), supplemented with 10% fetal bovine serum (Gibco, 10270), 2 mM L-glutamine, and 1% penicillin/streptomycin solution (Sigma-Aldrich, G7513; P0781) at 37°C under 5% $CO_2$. Murine myoblast C2.7 cells (*61*), rat myoblast L6E9 cells (*62*), and human fibroblast–derived myoblast cells from an HD and a patient with LGMD2H were cultured in DMEM, supplemented with 20% fetal bovine serum, 2 mM L-glutamine, and 1% penicillin/streptomycin solution at 37°C under 5% $CO_2$. Myoblast differentiation was induced by culturing cells in DMEM supplemented with 2% horse serum (Life Technologies, 16050122), 2 mM L-glutamine, and 1% penicillin/streptomycin for an indicated amount of time. Fibroblasts from an HD and a patient with LGMD2H were provided by the Telethon Network of Genetic Biobanks project no. GTB12001. To prepare fibroblasts, a patient's skin biopsy was obtained after informed consent and approval of the Ethics Committee of the University of Ferrara. No cell lines used in this study were found in the database of commonly misidentified cell lines maintained by the International Cell Line Authentication Committee and National Center for Biotechnology Information biosample. Cells were screened for mycoplasma contamination by PCR (ABMgood, G238).

To evaluate autophagy, C2.7 cells and HD/LGMD2H-differentiated myoblasts were treated with 400 μM dexamethasone (Calbiochem, 265005) in the presence or absence of E64d/pepstatin A (5 μg/ml) (Santa Cruz Biotechnology, sc-201280A and sc-45036) or 5 nM Bafilomycin A1 (Sigma-Aldrich, B1793) or incubated with nutrient-deprived medium Earle's balanced salt solution (Sigma-Aldrich, E2888) for the indicated time, according to guidelines. The autophagy inhibitor 3MA (Sigma-Aldrich, M9281) was used at 5 mM.

### Myoblasts transdifferentiation

Myoblast preparation was obtained by transducing human fibroblasts from healthy or Trim32 mutant patients with the lentivirus cytomegalovirus (CMV) MyoD-ER(T) (Addgene) with a multiplicity of infection of 20 and treated with 1 μM 4OH-tamoxifen (Sigma-Aldrich, H7904)

to activate MyoD-ER(T). The transdifferentiation was confirmed by PCR analysis of MyoD and myogenin expression. Autophagy analysis was performed in the absence of 4OH-tamoxifen.

### Animal studies

*Trim32* KO mice were previously described (*22*). TRIM32 KO and WT mice were maintained and treated according to approved protocols and in accordance with the institutional and national guidelines and regulations (IP00001489) approved by the Oregon Health and Science University. To analyze the autophagy response to dexamethasone, 3-month-old mice ($n = 4$ for each genotype) were injected subcutaneously with dexamethasone sodium salt (5 mg/kg; Sigma-Aldrich, D-1756) and prepared in a saline solution (vehicle, 0.9% NaCl). The control group received an injection of saline solution (vehicle, 0.9% NaCl). Eight hours after injection, mice were sacrificed, and quadricep muscles were harvested and deep-frozen in liquid nitrogen before storing at −80°C for subsequent protein extraction. For immunoblotting analysis, frozen muscles were crushed into a fine powder with a hammer, resuspended in the extraction buffer (Coimmunoprecipitation Kit, Thermo Fisher Scientific, 14321D), supplemented with protease, phosphatase, and deubiquitinase inhibitors as described above, homogenized using a Dounce homogenizer, incubated at 4°C for 30 min, and centrifuged at 13,000 rpm for 10 min to remove debris. Same amounts of total protein (30 μg per well) were loaded on SDS–polyacrylamide gel electrophoresis (PAGE) for immunoblotting analysis.

### Transfection and viral infection

293 T cells were transiently transfected with expression vectors using the calcium phosphate method, as previously described (*32*). For retroviral production, packaging cells [293 gp/bsr (gag-pol/blasticidin S-resistant gene)] were cotransfected with 15 μg of retroviral vectors and 5 μg of pCMV-VSV-G using the calcium phosphate method. For lentiviral production, 293 T cells were cotransfected with 10 μg of lentiviral vectors, 2.5 μg of pCMV-VSV-G, and 7.5 μg of psPAX2 plasmid by using the calcium phosphate method. After 48 hours, the supernatant containing the retroviral or lentiviral particles was recovered, ultracentrifuged at 19,800 rpm on an SW28 rotor for 2 hours, and resuspended in phosphate-buffered saline (PBS) (500 μl for 20 ml of supernatant). Cells were infected with 80 μl of viral suspension in a medium supplemented with polybrene (4 μg/ml) for 8 hours. Two consecutive rounds of infections were performed to improve efficiency.

To establish *Trim32* KO cells for mutant complementation assays, C2.7 cells were transiently transfected with CRISPR-Cas9 vectors by Lipofectamine LTX and Plus Reagent (Invitrogen, 15338-100), as indicated by the supplier. Transduced cells were incubated with puromycin dihydrochloride (2.5 μg/μl; Santa Cruz Biotechnology, sc-108071) for only 48 hours to select transfected cells, where inactivation of Trim32 CRISPR-Cas9 has occurred, and then cultured in the absence of puromycin to avoid selecting cells with a stably integrated CRISPR-Cas9 vector.

### Plasmids

pCDNA3 hemagglutinin (HA)–Trim32 had been previously described (*10*). The HA-Trim32 mutants that correspond to human complementary DNA (cDNA) pathogenic Trim32 mutations were engineered with the QuickChange Site-Directed Mutagenesis Kit (StrateGene).

All retroviral constructs were based on a modified version of a pLPCX vector (Clontech) (*32*). pLPCX plasmids encoding FLAG- and MYC-WT AMBRA1, MYC-AMBRA1 mutants (amino acids 1 to 532, 533 to 751, and 761 to 1269), and FLAG–BECLIN 1 were previously described (*30*–*32*). pLPCX FLAG-TRIM32 and pLPCX TRIM32 were obtained by subcloning from pCDNA3 HA-TRIM32. pLPCX FLAG-TRIM32 deletion mutant RING/B-box (amino acids 1 to 136), coiled-coil domain (amino acids 136 to 326), NHL repeats (amino acids 327 to 653), and ΔNHL (amino acids 1 to 325) were created using the appropriate oligonucleotides and amplification, followed by in-frame insertion into the pLPCX FLAG vector. pCDNA3 HA-Trim32 C39S was generated by site-specific mutagenesis; pLPCX FLAG-TRIM32 C39S was obtained by subcloning from pCDNA3 HA-TRIM32 C39S. pLPCX FLAG-ULK1 and pLPCX MYC-ULK1 was obtained by subcloning from pcDNA3 Myc-tag ULK1 (*31*). pLPCX FLAG-ULK1 deletion mutants (amino acids 1 to 828 and 829 to 1050) were created using appropriate oligonucleotides and amplification, followed by in-frame insertion into the pLPCX FLAG vector. pRK5 HA-UBIQUITIN was obtained from Addgene (#17608). A CRISPR-Cas9 All-in-One lentiviral vector specific for human TRIM32 and murine TRIM32 [hTRIM32 single-guide RNA (sgRNA), K2465605; mTRIM32 sgRNA, K3452705] and control sgRNA (scramble sgRNA, K010) were purchased from ABMgood.

For stable murine Trim32 mRNA interference, two lentiviral *Trim32* mRNA–targeting pLKO.1 plasmids were used (TRCN0000040831 and TRCN0000040832; Sigma-Aldrich). For stable murine Ambra1 mRNA interference, two lentiviral *Ambra1* mRNA–targeting pLKO.1 plasmids were used (TRCN0000189905 and TRCN0000189940; Sigma-Aldrich). For stable human AMBRA1 mRNA interference, a lentiviral *AMBRA1* mRNA–targeting pLKO.1 plasmid was used (TRCN0000168652; Sigma-Aldrich). For stable murine *Nedd4L* mRNA interference, a lentiviral *Nedd4L* mRNA–targeting pLKO.1 plasmid was used (TRCN0000086870; Sigma-Aldrich). A pLKO.1 containing a nonmammalian shRNA was used as a negative control (Sigma-Aldrich).

### Antibodies

The primary antibodies used in this study were rabbit anti-HA antibody (Sigma-Aldrich, H6908), rabbit anti-FLAG antibody (Sigma-Aldrich, F7425), mouse anti-MYC antibody [Santa Cruz Biotechnology, sc-40 (9E10)], rabbit anti-MYC antibody (Millipore, 06-549), rabbit anti–BECLIN 1 [Santa Cruz Biotechnology, sc-11427 (H-300)], goat anti–BECLIN 1 [Santa Cruz Biotechnology, sc-10086 (D-18)], rabbit phospho–BECLIN 1 ($Ser^{15}$) [Cell Signaling Technology, 138255 and 84966 (D4B7R)], rabbit anti-ATG14 [Cell Signaling Technology, 96752 (D1A1N)], rabbit phospho-ATG14 [Cell Signaling Technology, 13155 (S29)], rabbit anti-NBR1 (Novus Biologicals, NBP1-71703), LC3 (Cell Signaling Technology, 27755), mouse anti–human AMBRA1 [Santa Cruz Biotechnology, sc-398204 (G6)], rabbit anti–human AMBRA1 (Novus Biologicals, 26190002), rabbit anti-mouse Ambra1 (Millipore, ABC131), mouse anti–multi ubiquitin (MBL International, ST1200), rabbit anti–K63-linked ubiquitin (Millipore, 05-1308), rabbit anti–K48-linked ubiquitin (Millipore, 05-1307), rabbit anti-ULK1 [Santa Cruz Biotechnology, sc-33183 (H240)], rabbit anti-ULK1 [Cell Signaling Technology, 80545 (D8H5)], rabbit anti-TRIM32 (Thermo Fisher Scientific, PA5-22316), rabbit anti–phospho-VPS34 ($Ser^{249}$) (Cell Signaling Technology, 138575), rabbit anti-VPS34 (Life Technologies, 382100), mouse

anti-GAPDH (glyceraldehyde-3-phosphate dehydrogenase) (Millipore, CB1001), and mouse monoclonal myosin heavy chain antibody MF20 (Novus Biologicals, MAB4470).

### Immunoprecipitation and immunoblotting assays

Coimmunoprecipitation was performed by lysing cells in tris buffer [10 mM tris (pH 8.0) (Santa Cruz Biotechnology, sc-3715A), 150 mM NaCl (Sigma-Aldrich, S7653), 10% glycerol (Sigma-Aldrich, G7757), 0.5% NP-40 (Sigma-Aldrich, 56741)] or in CHAPS buffer, in the case of ULK1, as previously described (*31*). Radioimmunoprecipitation assay (RIPA) buffer [150 mM NaCl (Sigma-Aldrich, S7653), 1% NP-40 (Sigma-Aldrich, 56741), 0.5% deoxycholic acid (MP Biomedicals, 101496), 0.1% SDS (Sigma-Aldrich, L3771), 50 mM tris (pH 8.0) (Santa Cruz Biotechnology, sc-3715A), and 2 mM $MgCl_2$ (Sigma-Aldrich, M8266)] was used to analyze ubiquitination levels of immunoprecipitated proteins and for immunoblotting assays. Lysis buffer was complemented with protease and phosphatase inhibitors [Protease Inhibitor Cocktail plus (Sigma-Aldrich, P8340), 5 mM sodium fluoride (Sigma-Aldrich, S-7920), 0.5 mM sodium orthovanadate (Sigma-Aldrich, S6508), 1 mM sodium molibdate (Sigma-Aldrich, S-6646), 50 mM 2-chloroacetamide (Sigma-Aldrich, C0267), 2 mM 1,10-phenanthroline monohydrate (Sigma-Aldrich, 320056), and 0.5 mM phenylmethylsulfonyl fluoride (Sigma-Aldrich, P7626)]. Coimmunoprecipitation was performed with 1 mg of protein extracts from transfected cells or 3 mg in the case of endogenous proteins assays. For endogenous protein immunoprecipitation, protein extracts were incubated overnight with 2 μg of antibody, and immunocomplexes were recovered using 25 μl of Protein A Sepharose (GE Healthcare, GE 17-1279-01). For immunoprecipitation of overexpressed tagged proteins, protein extracts were incubated with 25 μl of anti-FLAG, anti-HA, or anti-MYC antibodies conjugated to agarose beads (Sigma-Aldrich: A22220, A2095, and A7470, respectively) for 2 hours. To test the covalent binding of polyubiquitin chains to ULK1, in the first-round immunoprecipitation assay, cell extracts were prepared as described above, and then, lysates were incubated with the anti-FLAG antibody conjugated to agarose beads for 2 hours. Immunoprecipitates were washed three times with RIPA buffer. Before the second-round immunoprecipitation assay, the immunoprecipitates were denatured by boiling for 5 min at 95°C in the lysis buffer containing 1% SDS. The eluates were then diluted 1:10 with lysis buffer and reimmunoprecipitated with the anti-FLAG antibody conjugated to agarose beads for 2 hours.

Immunocomplexes were separated on NuPAGE bis-tris gels (Life Technologies, 4 to 12% EA0378BOX and 3 to 8% NW04120BOX) and electroblotted onto nitrocellulose (Whatman Amersham, 10600041) or polyvinylidene difluoride (Millipore, IPVH20200) membranes. Detection was achieved using horseradish peroxidase–conjugated secondary antibodies [anti-goat 705-036-147, anti-rabbit 711-036-152, and anti-mouse 715-036-150 (Jackson ImmunoResearch Laboratories)] and enhanced chemiluminesence (ECL) [Immobilon Classico WBLUC0500 and Immobilon Crescendo Western HRP substrate WBLUR0500 (Millipore)]. Signals were acquired using Amersham Hyperfilm ECL (GE Healthcare, 28-9068-37) or a ChemiDoc imaging system.

### Ubiquitination assay

293 T cells were independently transfected with plasmids encoding MYC-ULK1 or FLAG-TRIM32. Forty-eight hours later, cells were lysed in RIPA buffer for ULK1 purification and tris buffer for TRIM32 immunoprecipitation, both containing protease inhibitors, as previously indicated. Lysates were cleared by centrifugation and subjected to immunoprecipitation for 2 hours using agarose-coupled antibodies against MYC or FLAG tags. TRIM32 protein was eluted for 1 hour by means of FLAG peptide (Sigma-Aldrich, F3290) at 400 ng/μl in the 1X Ubiquitin Conjugation Reaction Buffer (Boston Biochem, B-70). The ubiquitination assays were performed in 100 μl of reaction volume, combining 20 μl of immunopurified MYC-ULK1 bound to agarose-beaded Myc antibody, 20 μl of eluted TRIM32, and the following recombinant components: 100 nM E1 Ub–activating enzyme (Ube1; Boston Biochem, E-305), 1 μM E2 Ub–conjugating enzyme (Ube2N; Boston Biochem, E2-664), and 50 μM HA-ubiquitin (Boston Biochem, U-110) resuspended in Ubiquitin Reconstitution Buffer (Boston Biochem, B-90). In some in vitro ubiquitination experiments, recombinant ULK1 protein (SignalChem, U01-11G) was used instead of the immunopurified one. The reaction was performed in 1X Ubiquitin Conjugation Reaction Buffer, supplemented with $Mg^{2+}$–adenosine triphosphate (Boston Biochem, B-20) at 2 mM and incubated at 30°C for 2 hours in a rocking platform. When indicated, a denaturation step was added as previously described, followed by a reimmunoprecipitation of ULK1 using the rabbit anti-ULK1 H240 antibody (Santa Cruz Biotechnology, sc-33183). The incorporation of ubiquitin was analyzed by immunoblotting using rabbit anti-HA antibody (Sigma-Aldrich, H6908) to detect HA-ubiquitin.

### Real-time PCR

Real-time PCR was performed, as previously described (*63*). Briefly, RNA was extracted by using a TRIzol reagent (Invitrogen, 15596-018). cDNA synthesis was generated using a reverse transcription kit (Promega, A3500), according to the manufacturer's recommendations. qPCR reactions were performed with the Rotor-Gene 6000 (Corbett Research Ltd.) thermocycler. The Maxima SYBR Green/ROX qPCR Master Mix (Thermo Fisher Scientific, K0253) was used to produce fluorescently labeled PCR products during repetitive cycling of the amplification reaction, and the melting curve protocol was used to check for probe specificity, as described previously (*30*). The following primer sets for all amplicons were designed using the Primer-Express 1.0 Software System (Roche): mouse MuRF1 forward (5′-CCAAGGAAAGAGCAGTATGG-3′) and reverse (5′-GCAGCTCTCTGGGTTATTG-3′), mouse p62 forward (5′-TGAAACATGGACACTTTGGCTGGC-3′) and reverse (5′-ACATTGGGATCTTCTGGTGGAGCA-3′), mouse NBR1 forward (5′-GAGATGAGAGGGAGGAGATT-3′) and reverse (5′-CTTCAGAGGAAGCAGAAGAC-3′), mouse GAPDH forward (5′-TTCAACGGCACAGTCAAG-3′) and reverse (5′-CCAGTAGACTCCACGACATA-3′), human MYOD forward (5′-CACAACGGACGACTTCTATG-3′) and MYOD reverse (5′-GTGCTCTTCGGGTTTCAG-3′), human MYOG forward (5′-GCGTGTAAGGTGTGTAAGAG-3′) and MYOG reverse (5′-GCCTCATTCACCTTCTTGAG-3′), and human GAPDH forward (5′-CGCTTCGCTCTCTGCTCCT-3′) and reverse (5′-CCGTTGACTCCGACCTTCAC-3′).

### Flow cytometry

Staining for mitochondria was performed by incubating differentiated C2.7 cells with 5 μM CellROX Deep Red Reagent (Thermo Fisher Scientific, C10422), following the manufacturer's protocols, and directly analyzed without fixing. Cell analysis was performed using FACScan (Becton-Dickinson).

### Muscle tissue analysis by fluorescent microscopy

To analyze the autophagy response to dexamethasone, 6-month-old mice ($n$ = 4 for each genotype) were injected subcutaneously with dexamethasone sodium salt (5 mg/kg; Sigma-Aldrich, D-1756) and prepared in a saline solution (vehicle, 0.9% NaCl). The control group received an injection of saline solution (vehicle, 0.9% NaCl). Twenty-four hours after injection, mice were sacrificed, and quadriceps were fixed with 4% formaldehyde for 24 hours at room temperature, and after dehydration with a series of alcohol-xylene dilutions, the tissue was embedded in paraffin and cut into 7-μm sections. Sections were then dewaxed and boiled for 8 min in preheated 10 mM citric acid retrieval buffer (pH 6.0). Sections were subsequently blocked in PBS containing 1% goat serum and 0.4% Triton X-100 for 1 hour before the primary antibody incubation in PBS containing 0.1% Tween 20 overnight at 4°C. Nuclei were stained with Hoechst 33342 (Sigma-Aldrich) during the incubation with the secondary antibody in PBS containing 0.1% Tween at room temperature for 1 hour. Fluorescent microscopy was performed at room temperature using the DeltaVision RT fluorescence microscope (Applied Precision, Issaquah, WA) equipped with a CoolSNAP HQ camera (Photometrix, Kew, Australia). Images were generated by collecting stacks of images with focal planes 0.30 μm apart and subsequently deconvolved using the SoftWoRx software (Applied Precision). The following antibodies were used: rabbit anti-LC3 (PM036; MBL International, Woburn, MA), guinea pig anti-p62 (GP62-C; Progen, Darra, Australia), Alexa Fluor 568–conjugated goat anti–guinea pig immunoglobin G (IgG; Thermo Fisher Scientific, A-11075), Alexa Fluor 488–cojugated goat anti-rabbit IgG (H + L) (Thermo Fisher Scientific, A27034).

### Electron microscopy

Differentiated C2.7 cells carrying control or TRIM32-targeting shRNA were incubated with 400 μM dexamethasone for 4 hours. Cells were fixed before and after dexamethasone treatment by direct addition of 5% glutaraldehyde (Merck Millipore, 1042390250) and 4% paraformaldehyde (Sigma-Aldrich, 441244) in 0.1 M cacodylate buffer (pH 7.4; Sigma-Aldrich, 20840-100G-F) to the culture medium. After a 20-min incubation at room temperature, the fixation solution was replaced by 2.5% glutaraldehyde and 2% paraformaldehyde in 0.1 M cacodylate buffer (pH 7.4), and fixation was prolonged overnight. Cells were then embedded in EPON resin [for 25 ml, 12 g of glycid ether (SERVA, 21045.02), 8 g of 2-dodecenysuccinic acid anhydride (SERVA, 20755.02), 5 g of methylnadic anhydride (SERVA, 29452.02), and 560 μl of *N*-benzyldimethylamine (Electron Miscroscopy Sciences, 11400-25)]. Subsequently, 55-nm sections were cut and stained with uranyl acetate and lead citrate. Cell sections were examined using an 80-kV CM100 transmission electron microscope (Phillips). Three different grids with sections obtained from the same preparations were statistically evaluated. For every grid, the average number of degradative compartments (amphisomes, autolysosomes, and lysosomes) per cell section was determined by counting 25 randomly selected cell profiles.

### Statistical analysis

Statistical analysis of electron miscroscopy data was analyzed using the Mann-Whitney test (independent samples and two-sided; GraphPad). Statistical analysis of immunoblotting, PCR, and fluorescence-activated cell sorting (FACS) data were performed using unpaired, two-tailed Student's $t$ test (Excel software). Values are shown as means ± SD of at least three independent experiments. $P$ values <0.05 were marked by an asterisk. Densitometric analysis of immunoblots was performed using the Adobe Photoshop software. The control ratio was arbitrarily defined as 1.00. Normal distribution was assumed on the basis of the appearance of the data, since $n < 5$. No statistical method was used to predetermine sample size for animal studies. The animal experiments were not randomized. The investigators were not blinded to allocation during experiments and outcome assessment. No exclusion criteria were applied to exclude samples or animals from analysis.

## SUPPLEMENTARY MATERIALS

Supplementary material for this article is available at http://advances.sciencemag.org/cgi/content/full/5/5/eaau8857/DC1

Fig. S1. AMBRA1, but not TRIM32, is required for basal autophagy in myoblast cells.
Fig. S2. Role of TRIM32 and AMBRA1 in autophagy induction by atrophic stimuli in muscle cells.
Fig. S3. Analysis of autophagy defects in TRIM32 silenced myoblasts.
Fig. S4. Role of Trim32 in autophagy induction by nutrient starvation in muscle cells.
Fig. S5. Analysis of autophagy defects in Trim32$^{-/-}$ mice.
Fig. S6. Analysis of MuRF1 and ROS levels in dexamethasone-treated muscle cells.
Fig. S7. Characterization of the proautophagic properties of TRIM32.
Fig. S8. Regulation of ULK1 activity by NEDD4L and TRIM32.
Fig. S9. Characterization of autophagy properties of C2.7 cells expressing TRIM32 pathological mutants.
Fig. S10. Defective autophagy induction in human and murine myoblast cells expressing TRIM32 pathological mutants.

## REFERENCES AND NOTES


1. L. Galluzzi, F. Pietrocola, B. Levine, G. Kroemer, Metabolic control of autophagy. *Cell* **159**, 1263–1276 (2014).
2. N. Mizushima, M. Komatsu, Autophagy: Renovation of cells and tissues. *Cell* **147**, 728–741 (2011).
3. A. M. K. Choi, S. W. Ryter, B. Levine, Autophagy in human health and disease. *N. Engl. J. Med.* **368**, 651–662 (2013).
4. M. Sandri, L. Coletto, P. Grumati, P. Bonaldo, Misregulation of autophagy and protein degradation systems in myopathies and muscular dystrophies. *J. Cell Sci.* **126**, 5325–5333 (2013).
5. P. Bonaldo, M. Sandri, Cellular and molecular mechanisms of muscle atrophy. *Dis. Model. Mech.* **6**, 25–39 (2013).
6. V. Carmignac, M. Svensson, Z. Körner, L. Elowsson, C. Matsumura, K. I. Gawlik, V. Allamand, M. Durbeej, Autophagy is increased in laminin α2 chain-deficient muscle and its inhibition improves muscle morphology in a mouse model of MDC1A. *Hum. Mol. Genet.* **20**, 4891–4902 (2011).
7. C. De Palma, F. Morisi, S. Cheli, S. Pambianco, V. Cappello, M. Vezzoli, P. Rovere-Querini, M. Moggio, M. Ripolone, M. Francolini, M. Sandri, E. Clementi, Autophagy as a new therapeutic target in Duchenne muscular dystrophy. *Cell Death Dis.* **5**, e1363 (2014).
8. P. Grumati, L. Coletto, P. Sabatelli, M. Cescon, A. Angelin, E. Bertaggia, B. Blaauw, A. Urciuolo, T. Tiepolo, L. Merlini, N. M. Maraldi, P. Bernardi, M. Sandri, P. Bonaldo, Autophagy is defective in collagen VI muscular dystrophies, and its reactivation rescues myofiber degeneration. *Nat. Med.* **16**, 1313–1320 (2010).
9. M. Chrisam, M. Pirozzi, S. Castagnaro, B. Blaauw, R. Polishchuck, F. Cecconi, P. Grumati, P. Bonaldo, Reactivation of autophagy by spermidine ameliorates the myopathic defects of collagen VI-null mice. *Autophagy* **11**, 2142–2152 (2015).
10. A. Reymond, G. Meroni, A. Fantozzi, G. Merla, S. Cairo, L. Luzi, D. Riganelli, E. Zanaria, S. Messali, S. Cainarca, A. Guffanti, S. Minucci, P. G. Pelicci, A. Ballabio, The tripartite motif family identifies cell compartments. *EMBO J.* **20**, 2140–2151 (2001).
11. M. G. Koliopoulos, D. Esposito, E. Christodoulou, I. A. Taylor, K. Rittinger, Functional role of TRIM E3 ligase oligomerization and regulation of catalytic activity. *EMBO J.* **35**, 1204–1218 (2016).
12. V. Nigro, M. Savarese, Genetic basis of limb-girdle muscular dystrophies: The 2014 update. *Acta Myol.* **33**, 1–12 (2014).
13. E. Kudryashova, J. Wu, L. A. Havton, M. J. Spencer, Deficiency of the E3 ubiquitin ligase TRIM32 in mice leads to a myopathy with a neurogenic component. *Hum. Mol. Genet.* **18**, 1353–1367 (2009).
14. E. Kudryashova, A. Struyk, E. Mokhonova, S. C. Cannon, M. J. Spencer, The common missense mutation D489N in TRIM32 causing limb girdle muscular dystrophy 2H leads to loss of the mutated protein in knock-in mice resulting in a *Trim32*-null phenotype. *Hum. Mol. Genet.* **20**, 3925–3932 (2011).
15. A. P. Chiang, J. S. Beck, H.-J. Yen, M. K. Tayeh, T. E. Scheetz, R. E. Swiderski, D. Y. Nishimura, T. A. Braun, K.-Y. A. Kim, J. Huang, K. Elbedour, R. Carmi, D. C. Slusarski, T. L. Casavant,

E. M. Stone, V. C. Sheffield, Homozygosity mapping with SNP arrays identifies *TRIM32*, an E3 ubiquitin ligase, as a Bardet-Biedl syndrome gene (*BBS11*). *Proc. Natl. Acad. Sci. U.S.A.* **103**, 6287–6292 (2006).
16. E. Lazzari, G. Meroni, TRIM32 ubiquitin E3 ligase, one enzyme for several pathologies: From muscular dystrophy to tumours. *Int. J. Biochem. Cell Biol.* **79**, 469–477 (2016).
17. E. Kudryashova, D. Kudryashov, I. Kramerova, M. J. Spencer, Trim32 is a ubiquitin ligase mutated in limb girdle muscular dystrophy type 2H that binds to skeletal muscle myosin and ubiquitinates actin. *J. Mol. Biol.* **354**, 413–424 (2005).
18. S. Cohen, B. Zhai, S. P. Gygi, A. L. Goldberg, Ubiquitylation by Trim32 causes coupled loss of desmin, Z-bands, and thin filaments in muscle atrophy. *J. Cell Biol.* **198**, 575–589 (2012).
19. S. Cohen, D. Lee, B. Zhai, S. P. Gygi, A. L. Goldberg, Trim32 reduces PI3K-Akt-FoxO signaling in muscle atrophy by promoting plakoglobin-PI3K dissociation. *J. Cell Biol.* **204**, 747–758 (2014).
20. E. Kudryashova, I. Kramerova, M. J. Spencer, Satellite cell senescence underlies myopathy in a mouse model of limb-girdle muscular dystrophy 2H. *J. Clin. Invest.* **122**, 1764–1776 (2012).
21. V. Saccone, M. Palmieri, L. Passamano, G. Piluso, G. Meroni, L. Politano, V. Nigro, Mutations that impair interaction properties of TRIM32 associated with limb-girdle muscular dystrophy 2H. *Hum. Mutat.* **29**, 240–247 (2008).
22. S. Nicklas, A. Otto, X. Wu, P. Miller, S. Stelzer, Y. Wen, S. Kuang, K. Wrogemann, K. Patel, H. Ding, J. C. Schwamborn, TRIM32 regulates skeletal muscle stem cell differentiation and is necessary for normal adult muscle regeneration. *PLOS ONE.* **7**, e30445 (2012).
23. E. I. Mokhonova, N. K. Avliyakulov, I. Kramerova, E. Kudryashova, M. J. Haykinson, M. J. Spencer, The E3 ubiquitin ligase TRIM32 regulates myoblast proliferation by controlling turnover of NDRG2. *Hum. Mol. Genet.* **24**, 2873–2883 (2015).
24. S. Chauhan, S. Kumar, A. Jain, M. Ponpuak, M. H. Mudd, T. Kimura, S. W. Choi, R. Peters, M. Mandell, J.-A. Bruun, T. Johansen, V. Deretic, TRIMs and Galectins globally cooperate and TRIM16 and Galectin-3 co-direct autophagy in endomembrane damage homeostasis. *Dev. Cell* **39**, 13–27 (2016).
25. M. Antonioli, M. Di Rienzo, M. Piacentini, G. M. Fimia, Emerging mechanisms in initiating and terminating autophagy. *Trends Biochem. Sci.* **42**, 28–41 (2017).
26. C. Fusco, B. Mandriani, M. Di Rienzo, L. Micale, N. Malerba, D. Cocciadiferro, E. Sjøttem, B. Augello, G. M. Squeo, M. T. Pellico, A. Jain, T. Johansen, G. M. Fimia, G. Merla, TRIM50 regulates Beclin 1 proautophagic activity. *Biochim. Biophys. Acta* **1865**, 908–919 (2018).
27. M. A. Mandell, A. Jain, J. Arko-Mensah, S. Chauhan, T. Kimura, C. Dinkins, G. Silvestri, J. Münch, F. Kirchhoff, A. Simonsen, Y. Wei, B. Levine, T. Johansen, V. Deretic, TRIM proteins regulate autophagy and can target autophagic substrates by direct recognition. *Dev. Cell* **30**, 394–409 (2014).
28. T. Kimura, M. Mandell, V. Deretic, Precision autophagy directed by receptor regulators— Emerging examples within the TRIM family. *J. Cell Sci.* **129**, 881–891 (2016).
29. Q. Yang, T.-T. Liu, H. Lin, M. Zhang, J. Wei, W.-W. Luo, Y.-H. Hu, B. Zhong, M.-M. Hu, H.-B. Shu, TRIM32-TAX1BP1-dependent selective autophagic degradation of TRIF negatively regulates TLR3/4-mediated innate immune responses. *PLOS Pathog.* **13**, e1006600 (2017).
30. G. M. Fimia, A. Stoykova, A. Romagnoli, L. Giunta, S. Di Bartolomeo, R. Nardacci, M. Corazzari, C. Fuoco, A. Ucar, P. Schwartz, P. Gruss, M. Piacentini, K. Chowdhury, F. Cecconi, Ambra1 regulates autophagy and development of the nervous system. *Nature* **447**, 1121–1125 (2007).
31. F. Nazio, F. Strappazzon, M. Antonioli, P. Bielli, V. Cianfanelli, M. Bordi, C. Gretzmeier, J. Dengjel, M. Piacentini, G. M. Fimia, F. Cecconi, mTOR inhibits autophagy by controlling ULK1 ubiquitylation, self-association and function through AMBRA1 and TRAF6. *Nat. Cell Biol.* **15**, 406–416 (2013).
32. S. Di Bartolomeo, M. Corazzari, F. Nazio, S. Oliverio, G. Lisi, M. Antonioli, V. Pagliarini, S. Matteoni, C. Fuoco, L. Giunta, M. D'Amelio, R. Nardacci, A. Romagnoli, M. Piacentini, F. Cecconi, G. M. Fimia, The dynamic interaction of AMBRA1 with the dynein motor complex regulates mammalian autophagy. *J. Cell Biol.* **191**, 155–168 (2010).
33. P. Xia, S. Wang, G. Huang, Y. Du, P. Zhu, M. Li, Z. Fan, RNF2 is recruited by WASH to ubiquitinate AMBRA1 leading to downregulation of autophagy. *Cell Res.* **24**, 943–958 (2014).
34. M. Antonioli, F. Albiero, F. Nazio, T. Vescovo, A. B. Perdomo, M. Corazzari, C. Marsella, P. Piselli, C. Gretzmeier, J. Dengjel, F. Cecconi, M. Piacentini, G. M. Fimia, AMBRA1 interplay with cullin E3 ubiquitin ligases regulates autophagy dynamics. *Dev. Cell* **31**, 734–746 (2014).
35. C. Van Humbeeck, T. Cornelissen, H. Hofkens, W. Mandemakers, K. Gevaert, B. De Strooper, W. Vandenberghe, Parkin interacts with Ambra1 to induce mitophagy. *J. Neurosci.* **31**, 10249–10261 (2011).
36. A. Di Rita, A. Peschiaroli, P. D'Acunzo, D. Strobbe, Z. Hu, J. Gruber, M. Nygaard, M. Lambrughi, G. Melino, E. Papaleo, J. Dengjel, S. E. Alaoui, M. Campanella, V. Dötsch, V. V. Rogov, F. Strappazzon, F. Cecconi, HUWE1 E3 ligase promotes PINK1/PARKIN-independent mitophagy by regulating AMBRA1 activation via IKKα. *Nat. Commun.* **9**, 3755 (2018).
37. T. Skobo, F. Benato, P. Grumati, G. Meneghetti, V. Cianfanelli, S. Castagnaro, M. Chrisam, S. Di Bartolomeo, P. Bonaldo, F. Cecconi, L. D. Valle, Zebrafish *ambra1a* and *ambra1b* knockdown impairs skeletal muscle development. *PLOS ONE* **9**, e99210 (2014).
38. E. M. McMillan, J. Quadrilatero, Autophagy is required and protects against apoptosis during myoblast differentiation. *Biochem. J.* **462**, 267–277 (2014).
39. E. L. Eskelinen, F. Reggiori, M. Baba, A. L. Kovács, P. O. Seglen, Seeing is believing: The impact of electron microscopy on autophagy research. *Autophagy* **7**, 935–956 (2011).
40. E. Masiero, L. Agatea, C. Mammucari, B. Blaauw, E. Loro, M. Komatsu, D. Metzger, C. Reggiani, S. Schiaffino, M. Sandri, Autophagy is required to maintain muscle mass. *Cell Metab.* **10**, 507–515 (2009).
41. R. Troncoso, F. Paredes, V. Parra, D. Gatica, C. Vásquez-Trincado, C. Quiroga, R. Bravo-Sagua, C. López-Crisosto, A. E. Rodriguez, A. P. Oyarzún, G. Kroemer, S. Lavandero, Dexamethasone-induced autophagy mediates muscle atrophy through mitochondrial clearance. *Cell Cycle* **13**, 2281–2295 (2014).
42. R. Fang, C. Wang, Q. Jiang, M. Lv, P. Gao, X. Yu, P. Mu, R. Zhang, S. Bi, J.-M. Feng, Z. Jiang, NEMO–IKKβ are essential for IRF3 and NF-κB activation in the cGAS-STING pathway. *J. Immunol.* **199**, 3222–3233 (2017).
43. R. C. Russell, Y. Tian, H. Yuan, H. W. Park, Y.-Y. Chang, J. Kim, H. Kim, T. P. Neufeld, A. Dillin, K.-L. Guan, ULK1 induces autophagy by phosphorylating Beclin-1 and activating VPS34 lipid kinase. *Nat. Cell Biol.* **15**, 741–750 (2013).
44. D. F. Egan, M. G. H. Chun, M. Vamos, H. Zou, J. Rong, C. J. Miller, H. J. Lou, D. Raveendra-Panickar, C.-C. Yang, D. J. Sheffler, P. Teriete, J. M. Asara, B. E. Turk, N. D. P. Cosford, R. J. Shaw, Small molecule inhibition of the autophagy kinase ULK1 and identification of ULK1 substrates. *Mol. Cell* **59**, 285–297 (2015).
45. F. Nazio, M. Carinci, C. Valacca, P. Bielli, F. Strappazzon, M. Antonioli, F. Ciccosanti, C. Rodolfo, S. Campello, G. M. Fimia, C. Sette, P. Bonaldo, F. Cecconi, Fine-tuning of ULK1 mRNA and protein levels is required for autophagy oscillation. *J. Cell Biol.* **215**, 841–856 (2016).
46. M. Neri, R. Selvatici, C. Scotton, C. Trabanelli, A. Armaroli, D. De Grandis, N. Levy, F. Gualandi, A. Ferlini, A patient with limb girdle muscular dystrophy carries a TRIM32 deletion, detected by a novel CGH array, in compound heterozygosis with a nonsense mutation. *Neuromuscul. Disord.* **23**, 478–482 (2013).
47. B. A. Neel, Y. Lin, J. E. Pessin, Skeletal muscle autophagy: A new metabolic regulator. *Trends Endocrinol. Metab.* **24**, 635–643 (2013).
48. A. Vainshtein, P. Grumati, M. Sandri, P. Bonaldo, Skeletal muscle, autophagy, and physical activity: The ménage à trois of metabolic regulation in health and disease. *J. Mol. Med.* **92**, 127–137 (2014).
49. A. Ulbricht, S. Gehlert, B. Leciejewski, T. Schiffer, W. Bloch, J. Höhfeld, Induction and adaptation of chaperone-assisted selective autophagy CASA in response to resistance exercise in human skeletal muscle. *Autophagy* **11**, 538–546 (2015).
50. S. Cohen, J. A. Nathan, A. L. Goldberg, Muscle wasting in disease: Molecular mechanisms and promising therapies. *Nat. Rev. Drug Discov.* **14**, 58–74 (2015).
51. M. A. Egerman, D. J. Glass, Signaling pathways controlling skeletal muscle mass. *Crit. Rev. Biochem. Mol. Biol.* **49**, 59–68 (2014).
52. Z.-P. Xia, L. Sun, X. Chen, G. Pineda, X. Jiang, A. Adhikari, W. Zeng, Z. J. Chen, Direct activation of protein kinases by unanchored polyubiquitin chains. *Nature* **461**, 114–119 (2009).
53. R. Rajsbaum, G. A. Versteeg, S. Schmid, A. M. Maestre, A. Belicha-Villanueva, C. Martínez-Romero, J. R. Patel, J. Morrison, G. Pisanelli, L. Miorin, M. Laurent-Rolle, H. M. Moulton, D. A. Stein, A. Fernandez-Sesma, B. R. tenOever, A. García-Sastre, Unanchored K48-linked polyubiquitin synthesized by the E3-ubiquitin ligase TRIM6 stimulates the interferon-IKKε kinase-mediated antiviral response. *Immunity* **40**, 880–895 (2014).
54. P. Bharaj, Y. E. Wang, B. E. Dawes, T. E. Yun, A. Park, B. Yen, C. F. Basler, A. N. Freiberg, B. Lee, R. Rajsbaum, The matrix protein of Nipah virus targets the E3-ubiquitin ligase TRIM6 to inhibit the IKKε kinase-mediated type-I IFN antiviral response. *PLOS Pathog.* **12**, e1005880 (2016).
55. T. Pertel, S. Hausmann, D. Morger, S. Züger, J. Guerra, J. Lascano, C. Reinhard, F. A. Santoni, P. D. Uchil, L. Chatel, A. Bisiaux, M. L. Albert, C. Strambio-De-Castillia, W. Mothes, M. Pizzato, M. G. Grütter, J. Luban, TRIM5 is an innate immune sensor for the retrovirus capsid lattice. *Nature* **472**, 361–365 (2011).
56. G. A. Versteeg, S. Benke, A. García-Sastre, R. Rajsbaum, InTRIMsic immunity: Positive and negative regulation of immune signaling by tripartite motif proteins. *Cytokine Growth Factor Rev.* **25**, 563–576 (2014).
57. P. K. Paul, S. K. Gupta, S. Bhatnagar, S. K. Panguluri, B. G. Darnay, Y. Choi, A. Kumar, Targeted ablation of TRAF6 inhibits skeletal muscle wasting in mice. *J. Cell Biol.* **191**, 1395–1411 (2010).
58. H. Sun, Y. Gong, J. Qiu, Y. Chen, F. Ding, Q. Zhao, TRAF6 inhibition rescues dexamethasone-induced muscle atrophy. *Int. J. Mol. Sci.* **15**, 11126–11141 (2014).
59. V. Cianfanelli, C. Fuoco, M. Lorente, M. Salazar, F. Quondamatteo, P. F. Gherardini, D. De Zio, F. Nazio, M. Antonioli, M. D'Orazio, T. Skobo, M. Bordi, M. Rohde, L. D. Valle, M. Helmer-Citterich, C. Gretzmeier, J. Dengjel, G. M. Fimia, M. Piacentini,

S. Di Bartolomeo, G. Velasco, F. Cecconi, AMBRA1 links autophagy to cell proliferation and tumorigenesis by promoting c-Myc dephosphorylation and degradation. *Nat. Cell Biol.* **17**, 706 (2015).
60. S. Chauhan, M. A. Mandell, V. Deretic, IRGM governs the core autophagy machinery to conduct antimicrobial defense. *Mol. Cell* **58**, 507–521 (2015).
61. D. Yaffe, O. Saxel, Serial passaging and differentiation of myogenic cells isolated from dystrophic mouse muscle. *Nature* **270**, 725–727 (1977).
62. D. Yaffe, Retention of differentiation potentialities during prolonged cultivation of myogenic cells. *Proc. Natl. Acad. Sci. U.S.A.* **61**, 477–483 (1968).
63. G. Refolo, F. Ciccosanti, M. Di Rienzo, A. Basulto Perdomo, M. Romani, T. Alonzi, M. Tripodi, G. Ippolito, M. Piacentini, G. M. Fimia, Negative regulation of mitochondrial antiviral signaling protein-mediated antiviral signaling by the mitochondrial protein LRPPRC during hepatitis C virus infection. *Hepatology* **69**, 34–50 (2019).

**Acknowledgments:** We thank L. Gonzalez-Cano and J. C. Schwamborn (University of Luxembourg) for providing muscle samples for preliminary experiments and R. Maione and A. Musarò (University of Rome Sapienza) for providing C2.7 and L6E9 cells, respectively. We thank the Genomic Disorder Biobank and Telethon Network of Genetic Biobanks (Telethon Italy grant GTB12001G) for banking of biospecimens. **Funding:** This work was supported, in part, by grants from the Telethon Foundation (GEP12072 to G.M.F.), AIRC (IG2015 no. 17404 to G.M.F., IG2014 no.14078 to G.M., and IG2014 no. 15244 to M.P.), the Italian Ministry of University and Research (FIRB Accordi di Programma 2011, PRIN 2015 20152CB22L), the Italian Ministry of Health (Ricerca Corrente and Ricerca Finalizzata to G.M.F., M.P., and G.M.), Fondazione Fibrosi Cistica (Progetto FFC#8/2018 to M.P.), Regione Lazio (progetto "Gruppi di Ricerca" 2018 to M.P.), FRIAS COFUND Fellowship Programme (University of Freiburg, Germany) and People Programme (Marie Curie Actions) of the European Union's Seventh Framework Programme (FP/2007-2013) under REA grant agreement no. 609305 (to M.A.), Daunia Plast (to G.M.), and NIH/NIAMS R01 AR070645 (to Y.L. and M.K.-M.). F.R. is supported by grants from ZonMW VICI (016.130.606), ALW Open Programme (ALWOP.310), Marie Skłodowska-Curie Cofund (713660), Marie Skłodowska-Curie ITN (765912), and ZonMW TOP grant (91217002). M.M. is supported by an ALW Open Programme (ALWOP.355). I.O. is a recipient of an FEBS long-term postdoctoral fellowship. **Author contributions:** M.D.R. performed most of the experiments with crucial help from M.A. (proteomic screening and ubiquitination assays), C.F. and B.M. (generation of Trim32 constructs), M.T.P. (LGMD2H cell maintenance and preparation), G.R. (real-time PCR and RNA interference), M.C. (FACS analysis), F.G. and A.R. (autophagy flux analysis), and F.C. (retroviral and lentiviral production and infections). Y.L., R.D.L.T., H.D., I.O., and M.K.-M. performed the in vivo studies. M.M. and F.R. performed the electron microscopy studies. M.N. and A.F. provided LGMD2H fibroblasts. M.D. conducted the transdifferentiation of LGMD2H fibroblasts in myoblasts. M.D.R. and G.M.F. wrote the manuscript with the help and suggestions of F.R., G.M., and M.P. G.M., M.P., and G.M.F. conceived and designed the research. All authors discussed the results and commented on the manuscript. **Competing interests:** G.M. is a paid consultant for Takeda Pharmaceutical Company. The other authors declare that they have no competing interests. **Data and materials availability:** All data needed to evaluate the conclusions in the paper are present in the paper and/or the Supplementary Materials. Additional data related to this paper may be requested from the authors.

Submitted 25 July 2018
Accepted 21 March 2019
Published 8 May 2019
10.1126/sciadv.aau8857

**Citation:** M. Di Rienzo, M. Antonioli, C. Fusco, Y. Liu, M. Mari, I. Orhon, G. Refolo, F. Germani, M. Corazzari, A. Romagnoli, F. Ciccosanti, B. Mandriani, M. T. Pellico, R. De La Torre, H. Ding, M. Dentice, M. Neri, A. Ferlini, F. Reggiori, M. Kulesz-Martin, M. Piacentini, G. Merla, G. M. Fimia, Autophagy induction in atrophic muscle cells requires ULK1 activation by TRIM32 through unanchored K63-linked polyubiquitin chains. *Sci. Adv.* **5**, eaau8857 (2019).